IEEE Access
Multidisciplinary | Rapid Review | Open Access Journal

Received November 13, 2019, accepted November 27, 2019, date of publication December 2, 2019,
date of current version December 16, 2019.

Digital Object Identifier 10.1109/ACCESS.2019.2957014

Connectivity Influences on Nonlinear Dynamics in Weakly-Synchronized Networks: Insights From Rössler Systems, Electronic Chaotic Oscillators, Model and Biological Neurons

LUDOVICO MINATI[1,2,3], (Senior Member, IEEE), HIROYUKI ITO[4], (Member, IEEE), ALESSIO PERINELLI[5], LEONARDO RICCI[2,5], (Member, IEEE), LUCA FAES[6], (Senior Member, IEEE), NATSUE YOSHIMURA[4,7], YASUHARU KOIKE[4], AND MATTIA FRASCA[8], (Senior Member, IEEE)

[1]Tokyo Tech World Research Hub Initiative (WRHI), Institute of Innovative Research, Tokyo Institute of Technology, Yokohama 226-8503, Japan
[2]Center for Mind/Brain Science (CIMeC), University of Trento, 38123 Trento, Italy
[3]Complex Systems Theory Department, Institute of Nuclear Physics, Polish Academy of Sciences, 31-342 Kraków, Poland
[4]FIRST, Institute of Innovative Research, Tokyo Institute of Technology, Yokohama 226-8503, Japan
[5]Department of Physics, University of Trento, 38123 Trento, Italy
[6]Department of Engineering, University of Palermo, 90128 Palermo, Italy
[7]PRESTO, JST, Saitama 332-0012, Japan
[8]Department of Electrical, Electronic, and Computer Engineering (DIEEI), University of Catania, 95125 Catania, Italy

Corresponding author: Ludovico Minati (lminati@ieee.org)

The work of L. Minati was supported by the Tokyo Tech World Research Hub Initiative (WRHI), Institute of Innovative Research (IIR), Tokyo Institute of Technology, Tokyo, Japan.

ABSTRACT Natural and engineered networks, such as interconnected neurons, ecological and social networks, coupled oscillators, wireless terminals and power loads, are characterized by an appreciable heterogeneity in the local connectivity around each node. For instance, in both elementary structures such as stars and complex graphs having scale-free topology, a minority of elements are linked to the rest of the network disproportionately strongly. While the effect of the arrangement of structural connections on the emergent synchronization pattern has been studied extensively, considerably less is known about its influence on the temporal dynamics unfolding within each node. Here, we present a comprehensive investigation across diverse simulated and experimental systems, encompassing star and complex networks of Rössler systems, coupled hysteresis-based electronic oscillators, microcircuits of leaky integrate-and-fire model neurons, and finally recordings from in-vitro cultures of spontaneously-growing neuronal networks. We systematically consider a range of dynamical measures, including the correlation dimension, nonlinear prediction error, permutation entropy, and other information-theoretical indices. The empirical evidence gathered reveals that under situations of weak synchronization, wherein rather than a collective behavior one observes significantly differentiated dynamics, denser connectivity tends to locally promote the emergence of stronger signatures of nonlinear dynamics. In deterministic systems, transition to chaos and generation of higher-dimensional signals were observed; however, when the coupling is stronger, this relationship may be lost or even inverted. In systems with a strong stochastic component, the generation of more temporally-organized activity could be induced. These observations have many potential implications across diverse fields of basic and applied science, for example, in the design of distributed sensing systems based on wireless coupled oscillators, in network identification and control, as well as in the interpretation of neuroscientific and other dynamical data.

INDEX TERMS Attractor dimension, chaotic transition, complexity, electronic chaotic oscillator, entropy, network topology, neuronal culture, nodal strength, node degree, nonlinear dynamics, prediction error, Rössler system, Saito oscillator, stochastic dynamics, structural connectivity, synchronization.

I. INTRODUCTION

Our world is pervaded by natural and engineered networks which are remarkably diverse not only in their constituent elements and their behaviors, but also in size and spatial scale. Yet, many tend to show similar statistical features, for example in the organization of the structural connections; these are thought to arise from self-organization processes that are, at least to some extent, universal. For this reason, the interdisciplinary study of a property or phenomenon over

The associate editor coordinating the review of this manuscript and approving it for publication was Yong Chen.

different types of complex networks can be highly relevant in informing new design approaches and paradigms [1]. On the one hand, the investigation of naturally-occurring networks such as neurons in nervous systems, species in ecosystems, and proteins in organisms has received increasing attention over the last two decades [2], [3]. On the other, diverse areas of engineering are currently experiencing a strong thrust towards better understanding the collective properties of interacting devices such as terminals in wireless telecommunication networks [4], nodes in Internet-of-Things (IoT) infrastructures [5], loads and generators in power networks [6], and sensors in distributed sensing networks [7]. This trend reflects a need to more pervasively distribute automation and intelligence for better serving societal needs through higher flexibility and resilience delivered at lower power consumption.

In networks of coupled systems, the arrangement of the structural interconnections determines the possible interactions, in turn shaping the behaviors that can be displayed by the system as a whole: discovering how to induce and harvest collective behaviors purposefully towards solving specific problems may be viewed as one of the most significant challenges of our times [8], [9]. For example, considering the elementary but paradigmatic case of diffusively-coupled oscillators, the onset and stability of a synchronous trajectory common to all network units are related to the spectral properties of the Laplacian matrix representing the interactions [10], [11]. Also, the emergence of intricate synchrony patterns, characterized by clusters of units sharing a collective behavior, different from that of the other groups, is closely related to the layout of the structural connections, such as the existence of orbital and equitable partitions [12], [13]. Ultimately, results such as these have inspired and enabled the development of some techniques for controlling networks, wherein it is crucial to identify the topological properties that can be relied upon in deciding to which nodes the desired control law should be applied [14]–[17].

The bulk of literature in this area has focused on the relationship between structure and collective state, but complex systems often operate in regimes different than that. Consider, for instance, a network of oscillators that are not strongly synchronized: paradigmatic examples are found in biological nervous systems where, on the contrary, high synchrony generally corresponds to pathological states such as epileptic seizures [18]. Indeed, it is recognized that a delicate balance between information integration and differentiation is essential for the emergence of higher functions such as cognition and consciousness, and these clearly cannot be understood trivially in terms of a coherent state engulfing the entire brain [19], [20]. In networks of weakly-coupled elements, interactions still play a primary role, but their action in shaping the collective behavior is rather elusive and difficult to characterize, also due to the possibly long-range correlations which may be engendered by operation close to criticality [21]–[23]. Accordingly, efforts to develop control strategies face more significant difficulties and controversies in deciding which nodes to target and how global dynamics could be steered [24], [25]. Consequently, the many possible practical engineering applications of networks of weakly-coupled entities remain comparatively underdeveloped [26].

Because under situations of weak synchronization there is, by definition, considerable richness and diversity in the time-series recorded or simulated across the network nodes, it becomes interesting to attempt relating the dynamical features of activity unfolding locally within each node (representing, for example, an electronic oscillator, a neuron, an individual in an ecosystem, or another intelligent agent) with the topological features of its connectivity to the rest of the network. More specifically, since a scale-free distribution of the node degree hallmarks many complex networks [1], [24], and heterogeneity in the degree distribution has knowingly non-trivial effects on the onset of strongly-synchronized states [27], searching for distinctive features in the behavior of the most densely-connected 'hub' nodes appears to be a natural choice. The question can be approached in a complementary manner via measures based on nonlinear dynamics theory such as predictability (i.e., level of determinism) and fractal dimension of the attractor (i.e., geometrical complexity) [28], and through estimating information production, storage and transfer [29], [30].

To the authors' knowledge, limited data is available regarding the effect that the local connectivity of each coupled element, represented by node degree and nodal strength in binary and weighted graphs respectively, has on these aspects. It is, however, agreed that for instance network structure and dynamics in the brain are discernibly associated at both the local and global levels [31], [32]. In analyses of time-series representing intrinsic brain activity, it was found that, compared to the rest of the network, hub regions of the cortex exhibit stronger signatures indicative of low-dimensional deterministic, possibly chaotic, nonlinear dynamics. In the same study, an experimental transistor-based oscillator network was considered as a toy model, and transition to chaos was noted to selectively occur in the nodes which were hardwired to mimic hubs [33]. Another study simulating a network of Stuart-Landau oscillators instanced over a realistic human connectome reported a correspondence of the node degree with the relative phases and amplitudes of oscillations [34]. Recently, a more comprehensive analysis revealed an association between topological role and dynamics, such that high degree appears to be associated with lower levels of complexity across diverse systems [35]. Together, these results point to a possibly general relationship that seems worthy of additional consideration.

In the present contribution, we reveal across a broad range of scenarios the possibly intricate effects that the local connectivity, i.e., number and strength of connections, can have on the activity within each network node. We consider elementary topologies, namely stars, as well as diverse instances of complex networks whose members are subject to different coupling levels. Firstly, we address the case of systems

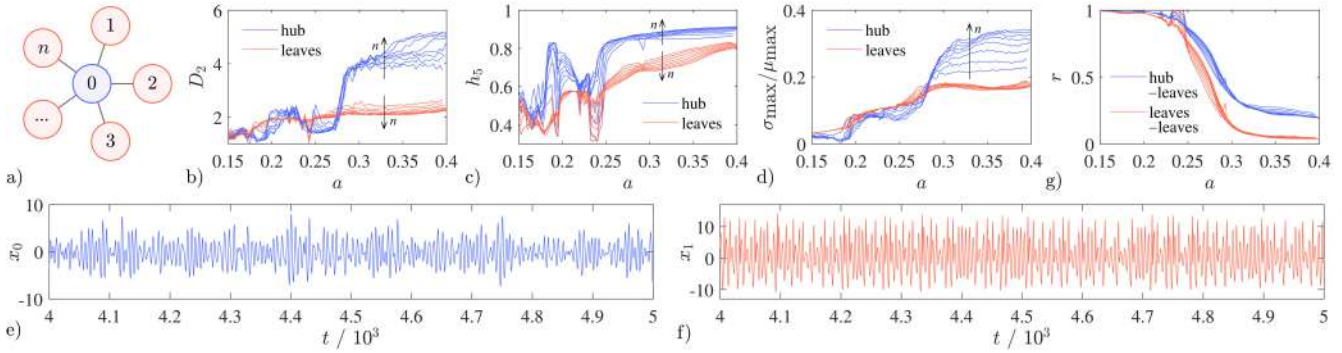

FIGURE 1. Effect of the bifurcation parameter a and node degree (number of leaves) n in star networks of Rössler systems. a) Network topology, where $n = 3, \ldots, 10$ and $u = 0.1$, b) Correlation dimension D_2 (blue: hub, red: average of leaves), c) Permutation entropy of adjacent local maxima h_5, d) Coefficient of variation for maxima amplitude fluctuations σ_{max}/μ_{max}, e) and f) Representative time-series for hub and leaf activity given $a = 0.35$, $n = 10$, and g) Phase synchronization r between the hub and leaves (blue) and among the leaves themselves (red). All measures derived from the x_j variables. Arrows denote the effect of increasing n.

that are primarily or wholly deterministic. In this context, we demonstrate via numerical simulations of Rössler chaotic units and experimental recordings of electronic nonlinear oscillators that high connectivity density can promote the onset of chaos and high-dimensional dynamics. However, when the coupling is more intense, the effect can be lost or even inverted. Secondly, we turn to systems wherein dynamics are markedly stochastic. In the latter settings, we show via numerical simulations of leaky integrate-and-fire neuronal circuits and recordings from in-vitro cultures of spontaneously-growing neuronal networks that high connectivity density can promote the local onset of nonlinear dynamics, that is, more predictable activity. Finally, the possible implications of these results on basic and applied science are discussed, both at the conceptual level and as regards the relevance for future applications of coupled oscillator networks across several engineering fields.

II. STAR NETWORKS OF RÖSSLER SYSTEMS

A. SIMULATION SETTINGS AND DYNAMICAL PARAMETERS

We firstly examine the case of Rössler systems diffusively coupled according to a star topology having n leaves (Fig. 1a). This case is paradigmatic because, on the one hand, the Rössler equations show considerable dynamical richness in spite of their low dimensionality and structural simplicity; they generate orbits which spiral in the vicinity of the x, y plane while, for suitable settings, spiking in the z dimension and twisting, giving rise to a characteristic chaotic attractor. As a function of the bifurcation parameter a, the level of folding can be controlled, whereby given $a = 0.1$ the dynamics are periodic (e.g., delineate a circle) and for $a \geq 0.2$ chaos ensues with increasingly rapid divergence and more complex trajectories [36]–[38]. On the other hand, the star topology plays a central role in graph theory, because it represents a simple situation wherein the nodes, namely the hub $j = 0$ and leaves $j = 1, \ldots, n$ dichotomously cluster into two categories having a different degree (number of connections, namely n and 1) and centrality. As such, it is the most elementary configuration exemplifying the effect of node degree. At the same time, star motifs are foundational in the construction of many emergent complex topologies, such as scale-free networks. The dynamics on star networks often allow some level of analytic solution, and their remarkable generative potential is exemplified by the observation of synchronization by dynamical relying, remote effects and even chimera states [39]–[45].

The following system was considered for $j = 0, \ldots, n$

$$\begin{cases} \dot{x}_j = -y_j - z_j + \sum_{k=0}^{n} g_{jk}(x_k - x_j) \\ \dot{y}_j = x_j + a y_j, \\ \dot{z}_j = b_j + z_j(x_j - c_j) \end{cases} \tag{1}$$

wherein

$$g_{jk} = \begin{cases} u & \text{if } (j = 0 \vee k = 0) \wedge j \neq k, \\ 0 & \text{otherwise} \end{cases} \tag{2}$$

fixing the secondary parameters to $b = 0.2$ and $c = 5.7$, and sweeping the bifurcation parameter $a \in [0.15, 0.40]$, running 100 simulations for star networks having $n = 3, \ldots, 10$ leaves. All parameters were set identically across the nodes and runs, while initial conditions were randomized, setting $x_j(0) = y_j(0) = 0$ and drawing $z_j(0) \in [-10, 10]$. The simulations were run until $t_{end} = 5 \times 10^3$, discarding the first 20% to allow initial transient stabilization. The system was integrated with variable step size using the Adams-Bashforth-Moulton family of formulas of orders 1-12 [46], setting the relative and absolute tolerances to 10^{-3} and 10^{-6}, respectively. A simulation was deemed to have diverged if $\max(x_j, y_j, z_j) > 10^3$ and thus aborted. A total of $N = 100$ networks were simulated for each configuration, and average results are presented.

To gauge the effect of node degree on the complexity of the emergent dynamics, we firstly reconstructed the phase-space of each network node j from its simulated time-series $x_j(t)$ by

means of time-delay embedding, with $x_j(t) = [x_j(t - \delta t(m - 2)), x_j(t - \delta t(m-1)), \ldots, x_j(t)]$ [47], wherein the embedding lag δt was set according to the first local minimum of the time-lag mutual information function [48], and the embedding dimension m was given by the lowest integer number yielding <5% of false nearest neighbors [49]. For attenuating bias due to temporal correlation between adjacent samples, the minimum neighbor time separation (Theiler window w) was set to twice the first local maximum of the space-time separation plot [50]. Unless stated otherwise, all nonlinear time-series analyses were carried out using the TISEAN package (ver. 3.0.1) [28], [51]. Predicated on the time-lag reconstruction, we estimated the geometrical complexity of the strange attractor by means of the correlation dimension D_2, as given by the Grassberger-Procaccia method [52]. In brief, D_2 was computed from the correlation sum

$$C(m, \epsilon) = \frac{1}{N_{\text{pairs}}} \sum_{j=m}^{N} \sum_{k<j-w} \Theta(\epsilon - |x_j - x_k|) \tag{3}$$

where $N_{\text{pairs}} = (N - m + 1)(N - m - w + 1)/2$ denotes the number of point pairs covered by the sums, and $\Theta(x)$ is the Heaviside step function. Over sufficiently small length scales ϵ, assuming that the embedding dimension m suitably exceeds the box-dimension of the underlying attractor, one should find

$$C(m, \epsilon) \propto \epsilon^{D_2}. \tag{4}$$

Here, over-embedding up to $2m$ was provided, the calculations were performed for 50,000 points interpolated at a fixed time-step twice the median variable step, and convergence of the estimated values of D_2 in m was estimated using a simple direct search method which also estimated the range of ϵ [53]. It should be borne in mind that this estimation method may negatively bias D_2 in the context of high-dimensional signals as might be expected here for large node degree n, nevertheless, it is widely adopted and understood [54].

To confirm and extend this analysis, a map-like account of the dynamics was also considered. After mean subtraction, all local maxima points, given by $\dot{x}(t) = 0$, $\ddot{x}(t) < 0$ and $x(t) > x(t \pm \delta t)$ with $\delta t = 10$ interpolated points, were extracted, yielding a corresponding step-wise amplitude time-series $\hat{x}_{\max}(i)$ having length l. Based on this representation, previously used to summarize chaotic dynamics, e.g., in Refs. [35] and [55], we computed another measure of complexity, based on information-theoretical rather than dynamical notions, namely, the permutation entropy. This is a robust non-parametric method, based on a purely ordinal representation of the data. Similarly to the case of D_2, an L-dimensional space was firstly constructed, made of the L-tuples $(u_1, \ldots, u_L) = (x_n, x_{n+1}, \ldots, x_{n+L-1})$. In this context, an L-tuple $(u_1, u_2, \ldots, u_L)$ is encoded as $S = (s_1, s_2, \ldots, s_L)$, wherein s_k denotes the ordinal position of u_k: in other words, the dynamics are encoded by ranks, based on the symbolic sequences of ascending and descending values. Provided the phase space is adequately filled, the permutation entropy is given by

$$H_m = -\sum_{j}^{m!} p_j \log_2 p_j, \tag{5}$$

wherein p_j denote the relative symbol frequencies, and which then can be normalized to give $h_m = H_m / \log_2 m! \in [0, 1]$ [56]. Here, the order (sequence length) was empirically set to $m = 5$, as this ensured that in the vast majority of cases the coverage criterion $5m! < l$ was met, but this setting is not critical [57]. In addition, from this map-like time-series the local maxima amplitude average $\mu_{\max}$ and standard deviation $\sigma_{\max}$ were calculated: their ratio $\sigma_{\max}/\mu_{\max}$ provided an immediate, intuitively-appealing additional measure of signal irregularity expressed in terms of the coefficient of variation [58]. To attenuate the effect of regular alternation of high and low cycles, e.g. due to period doubling, a 5-point moving average filter was applied.

Throughout Sec. II-IV, complexity is empirically measured via the correlation dimension D_2, which estimates the dimension of the possibly strange attractor, and via the permutation entropy h_5, which reflects the information content in a Shannonian sense. This is deemed acceptable therein, given that the systems under consideration are wholly or strongly deterministic, and non-triviality is thus considered only in reference to deviation from order and not from randomness. Other works consider measures of statistical complexity explicitly grounded on the thermodynamical notion of disequilibrium [35], [59], [60]. Some comparisons with the measure of statistical complexity S introduced in Ref. [35] (therein, C) are nevertheless provided in Sec. III and V. As regards the coefficient of variation, by construction it is insensitive to the temporal order of samples, thus, it only serves as an adjunct measure and cannot be formally considered a complexity index.

Lastly, it is necessary to quantify the level of synchronization, between the hub and the leaves, and among the leaves themselves. To this end, we focused on phase coherence because the entrainment of phases is the earliest indicator of emerging synchronization while a coupling strength is increased [61]. For a time-series $x_j(t)$, the corresponding analytic signal was calculated

$$\psi_j(t) = x_j(t) + i\tilde{x}_j(t) = A_j(t)e^{i\varphi_j(t)}, \tag{6}$$

where $i = \sqrt{-1}$, $\tilde{x}_j(t)$ denotes the Hilbert transform of $x_j(t)$

$$\tilde{x}_j(t) = \frac{1}{\pi}\text{p.v.}\left[\int_{-\infty}^{\infty} \frac{x_j(\tau)}{t - \tau} \mathrm{d}\tau\right], \tag{7}$$

and where p.v. represents the Cauchy principal value of the integral. From these complex-valued signals, for each node pair (j, k) the instantaneous relative phase could be obtained with

$$\Delta\varphi(t) = \arg[\psi_j(t)\overline{\psi}_k(t)], \tag{8}$$

finally yielding the corresponding phase-locking value

$$r = |\langle e^{i\Delta\varphi(t)}\rangle_t|. \tag{9}$$

B. EFFECTS OF NODE DEGREE AND COUPLING STRENGTH

With reference to Fig. 1a, let us consider the Rössler systems diffusively coupled according to a star topology having n leaves and, for now, a fixed coupling strength of $u = 0.1$. One firstly observes that, in the leaves, the correlation dimension increases only slowly with the bifurcation parameter a, settling and dwelling around $D_2^{(\text{leaves})} \approx 2$ for $a > 0.2$, without a clear effect of the hub node degree n (Fig. 1b). This level reflects that established for uncoupled Rössler systems [36]. In turn, it implies that the dynamics of the leaves are largely insensitive to the connectivity of the hub they are coupled with. For small values of the parameter a, the dynamics of the hub remain close to those of the leaves. However, by contrast, at around $a = 0.275$, the correlation dimension of the hub jumps to $D_2^{(\text{hub})} \approx 4$, signaling the emergence of high-dimensional dynamics. This result implies that, when the bifurcation parameter is sufficiently large, the two types of nodes in the star spontaneously develop markedly different dynamics. It is inherently a topological effect, given that all system parameters are set identically across the network. Unlike the leaves, towards the largest values of a, in the hub an influence of the node degree emerges, whereby the larger networks are associated with higher complexity of the underlying attractor.

From the map-like representation of successive local maxima amplitudes, one draws similar conclusions. While the effect of the bifurcation parameter a on the permutation entropy h_5 shows some differences compared to the above, a marked separation between the hub and the leaves is consistently present, whereby $h_5^{(\text{hub})} > h_5^{(\text{leaves})}$ (Fig. 1c). Here, the distinction becomes visible also at lower levels of a, i.e., $a = 0.2$. Further, though the effect of the hub node degree n appears more constrained, one finds that over a wide range of a, elevating n increases h_5 within the hub and lowers it within the leaves. Therefore, in larger networks the dynamics of the two node types become more differentiated. At the same time, the coefficient of variation $\sigma_{\max}/\mu_{\max}$ delineates a situation more similar to that revealed by the correlation dimension D_2 (Fig. 1d). In this case, the dynamics of the hub and leaves appear largely overlapping until $a = 0.275$; past this point, the variation within the hub becomes markedly larger, and a striking effect of the node degree n emerges within the same, while the leaves remain indifferent. A qualitative appreciation of the difference can be obtained by comparing representative time-series for the hub (Fig. 1e) and a leaf (Fig. 1f), showing smaller, comparatively more variable fluctuations in the former.

The above results need to be contextualized with regards to the level of synchronization, as indexed here by the phase coherence (Fig. 1g). For the chosen coupling strength $u = 0.1$, at levels of the bifurcation parameter such that chaoticity is not fully developed, namely $a < 0.2$, the entrainment is nearly perfect, with $r \approx 1$. A rapid decrease is thereafter observed in the region $0.2 < a < 0.3$, wherein chaoticity develops and the level of folding increases. For large values, namely $a > 0.3$, the level of synchronization drops to $r^{(\text{hub-leaves})} \approx 0.2$ between the hub and leaves, and $r^{(\text{leaves})} < 0.1$ among the leaves themselves, clearly hallmarking a regime of weak synchronization.

To gain further insight, it is necessary to study the system behavior while varying both the hub node degree (i.e., number of leaves) n and the coupling strength u. In doing so, we fix the bifurcation parameter at $a = 0.35$, based on the previous results which demonstrate that differentiated dynamics are clearly visible between the hub and leaves for this setting. In this scenario, the correlation dimension $D_2^{(\text{hub})}$ shows a non-monotonic trend: with stronger coupling, it firstly increases then eventually declines; this effect is particularly visible in the smaller networks, wherein simulations do not diverge until u is large (Fig. 2a). More precisely, already for the degenerate case $n = 1$, representing a node pair rather than a fully-developed star, one observes an initial increase from the value $D_2^{(\text{hub})} \approx 2$ expected for $u = 0$ (complete uncoupling), towards $D_2^{(\text{hub})} \approx 3.7$ for $u = 0.13$, finally followed by a decline back towards $D_2^{(\text{hub})} \approx 2$ for $u > 0.25$. Considering the case $n = 2$, representing a chain of nodes, one again observes an initial increase towards $D_2^{(\text{hub})} \approx 4$ for $u = 0.14$, followed by a slower decline towards $D_2^{(\text{hub})} \approx 2$ for $u > 0.5$. For the smallest proper star network and beyond, namely $n \geq 3$, the pattern is consistent, but the maximum correlation dimension of the hub notably increases with size, up to $D_2^{(\text{hub})} \approx 5$ for $n = 9$. Interestingly, the coupling strength at which it reaches its maximum value, namely $u \approx 0.1$, appears largely insensitive to the network size.

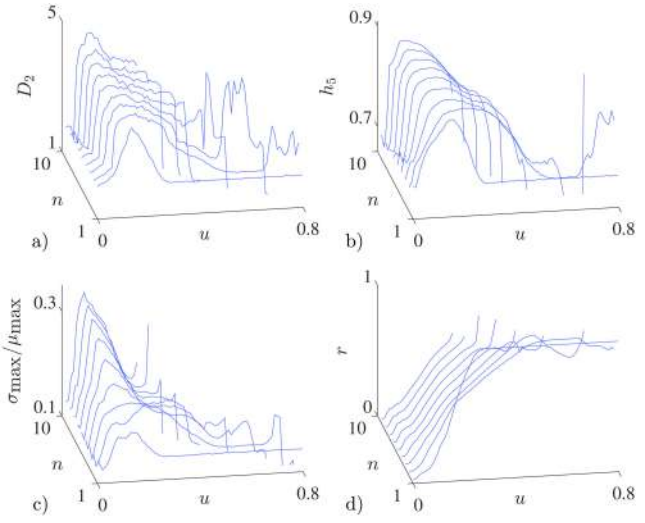

FIGURE 2. Effect of the node degree n and symmetric coupling strength u on the hub dynamics in star networks of Rössler systems, where $a = 0.35$. a) Correlation dimension D_2, b) Permutation entropy for local maxima amplitudes h_5, c) Coefficient of variation for maxima amplitude fluctuations $\sigma_{\max}/\mu_{\max}$, d) Phase synchronization r between the hub and leaves. All measures derived from the hub x_0 variable. Curves not shown where ≥ 50% of simulation runs diverged.

The other measures of complexity and irregularity provide largely consistent results. Namely, permutation entropy shows a non-monotonic trend over all network sizes, also peaking consistently around a coupling strength of $u \approx 0.1$.

The maximum value attained increases with the network size from $h_5^{(\mathrm{hub})} \approx 0.84$ at $n = 1$ up to $h_5^{(\mathrm{hub})} \approx 0.90$ at $n = 9$ (Fig. 2b). As before, the coefficient of variation provides an even more compelling picture; it follows a similar trend, but the maximum value increases more dramatically, from $\sigma_{\max}^{(\mathrm{hub})}/\mu_{\max}^{(\mathrm{hub})} \approx 0.2$ for $n = 1$ up to $\sigma_{\max}^{(\mathrm{hub})}/\mu_{\max}^{(\mathrm{hub})} \approx 0.33$ for $n = 9$ (Fig. 2c). Inherently, the phase coherence increases in $r \to 1$ for $u \to \infty$, even though for the larger networks divergence prevents this fully-synchronized state from being observed; since the Rössler systems in Eq. (1) are coupled to each other through their first state variables, they have a class III master stability function which, along with the fact that the largest eigenvalue of the Laplacian matrix of the star configuration is $\lambda_{n+1} = n+1$, is responsible for the unstable regime observed at large coupling. More importantly, at the coupling strength at which the strongest effect of the hub node degree is observed, namely $u \approx 0.1$, this measure remains consistently around $r^{(\text{hub-leaves})} \approx 0.2$, confirming a comparable situation of weak synchronization regardless of the number of leaves (Fig. 2d).

Thus far, these results indicate that the local connectivity can have rather prominent an effect in shaping the dynamics within each network node. For suitably large settings of the bifurcation parameter, a clear separation between the hub and the leaves emerges, with considerably higher-dimensional and more irregular dynamics arising in the former. The intensity of this effect depends, to some extent, on the number of leaves (i.e., node degree of the hub) n. However, more markedly, it depends on the coupling strength u: transition to a state of diversified dynamics is associated with, and plausibly requires, a situation of weak synchronization, wherein the energy exchange rate is sufficient for the leaves to collectively push the hub into more complex behavior, but there is not the emergence of a collective behavior engulfing the entire network.

A limited number of previous studies, albeit considering a different coupling mechanism, had addressed the effect of connectivity on the emergence of a collective chaotic state, including the need for a coupling strength within a bounded interval [62], [63]; compared to those earlier results, here we demonstrated in a rather more explicit manner the effects of degree and coupling strength, by means of investigating in detail the paradigmatic case of star networks. Because the coupled systems have, in principle, sufficient dimensionality to support hyperchaos, future work should explicitly derive the spectrum of Lyapunov exponents, to ascertain whether the observed higher-dimensional dynamics are associated with an increasing number of positive exponents; such an undertaking is beyond the scope of this work.

C. INFORMATION-THEORETICAL ANALYSIS AND ASYMMETRIC COUPLING

For shedding light into the temporal dynamics and the causative mechanisms underlying the differentiation of dynamics between the hub and leaves, it is necessary to analyze the network activity more deeply in terms of information generation, storage and transfer [30]. To this end, we herein consider the representative case of a star with $n = 5$ leaves and bifurcation parameter $a = 0.35$, while varying the coupling strength in $u \in [0, 0.4]$.

First, a bivariate scalar-driver analysis is performed, in virtue of the fact that each structural coupling is instanced between the hub and one leaf. The time-series of the leaf under consideration and the hub are described as realizing a 2-dimensional stochastic process $S = \{X, Y\}$, where X and Y are the scalar processes representing, respectively, the leaf and the hub. Then, denoting as X_t and Y_t the random variables obtained sampling the processes at the present time t, and as $X_t^- = [X_{t-1}, X_{t-2} \cdots]$, $Y_t^- = [Y_{t-1}, Y_{t-2} \cdots]$ the vector variables describing the past of the processes, the information dynamics within S are described as follows [30], [64]. The entropy of the hub process, defined as $H_Y = H(Y_t)$ and quantifying the amount of information contained in the current state of Y, is decomposed into $H_Y = S_Y + T_{X \to Y} + N_Y$, where $S_Y = I(Y_t; Y_t^-) = H(Y_t) - H(Y_t|Y_t^-)$ is the self-entropy of Y quantifying the information storage in the process, $T_{X \to Y} = I(Y_t; X_t^-|Y_t^-) = H(Y_t|Y_t^-) - H(Y_t|Y_t^-, X_t^-)$ is the transfer entropy from X to Y quantifying the information transferred from the leaf to the hub, and $N_Y = H(Y_t|X_t^-, Y_t^-)$ is the conditional entropy of Y given the past history of both nodes, quantifying the new information produced in the hub at each time point. In a fully symmetric way, the information contained in the leaf, $H_X = H(X_t)$ can be expanded as $H_X = S_X + T_{Y \to X} + N_X$ [65].

All measures were computed using the k-nearest neighbor method for entropy estimation [66], realizing a strategy to reduce the bias arising from the computation of entropies in variables having different dimension [67]. The estimator was implemented as detailed in Ref. [65] and applied considering $k = 10$ neighbors. In all calculations, the infinite-dimensional past of the processes was approximated by means of a uniform embedding scheme, i.e., $Y_n^- \approx [Y_{n-\tau}, Y_{n-2\tau}, \ldots, Y_{n-l\tau}]$, where the number of past components considered was $l = 5$, and the temporal spacing between lagged components, τ, was set to the lag past which the autocorrelation decays below $1/e$; to limit the computational load, only 20,000 points were considered. The precise settings of k, l and τ had limited impact on the analyses. To simplify their interpretation, T, S and N were normalized to the observed entropies of the corresponding target process H. The analysis was repeated separately for each leaf and averaged results are presented; in the following, "leaves" therefore denotes the average over all $j = 1, \ldots, n$ peripheral nodes considered individually.

In the uncoupling limit $u \to 0$, one has $D_2^{(\mathrm{hub})}, D_2^{(\mathrm{leaves})} \approx 2$ and $r \approx 0$ (Fig. 3a, b). Here, the transfer entropies between the hub and leaf are effectively null, i.e., $T_{X \to Y}, T_{Y \to X} \approx 0$ (Fig. 3c); furthermore, the amounts of stored and new information are the same, i.e., $S_Y/H_Y \approx S_X/H_X$ and $N_Y/H_Y \approx N_X/H_X$ (Fig. 3d, e), confirming the fact that all nodes initially have identical dynamics. The effects emerging for $u > 0$ are,

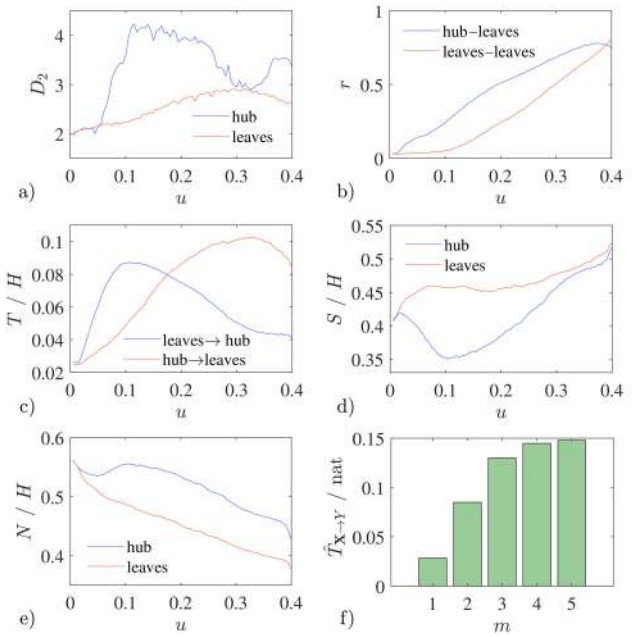

FIGURE 3. Information-theoretical perspective on the effect of symmetric coupling strength u in star networks of Rössler systems with $n = 5$ leaves and $a = 0.35$. a) Correlation dimension D_2 (blue: hub, red: average of leaves), b) Phase synchronization r with the hub (blue) and between the leaves (red), c) Transfer entropy T towards the hub and leaves (blue, red) normalized by corresponding observed entropy H (scalar-driver analysis), d) and e) Stored and new information, S and N, for hub and leaves (blue, red) normalized by the corresponding observed entropy H (scalar-driver analysis), f) Transfer entropy $\hat{T}$ towards the hub as a function of the number of leaves m included as sources of predictive information (vector-driver analysis). All measures derived from the x variable.

therefore, to be ascribed not to the intrinsic node dynamics, which were identical, but purely to the different position of the nodes in the network topology.

For small values of the coupling strength u, the transfer entropies start rising, markedly faster in the direction of the hub, $T_{X\to Y}/H_Y$, than of the leaf, $T_{Y\to X}/H_X$ (Fig. 3c). The amount of stored information sharply drops for the hub, S_Y/H_Y, whereas, by contrast, it increases for the leaves, S_X/H_X (Fig. 3d). Meanwhile, the amount of new information generated in the hub, N_Y/H_Y, transiently grows, whereas it monotonically declines for the leaves, N_X/H_X (Fig. 3e). Altogether, these measures point to the gradual emergence of greater dynamical complexity in the hub, which is reflected in a higher dimension $D_2^{(\text{hub})}$ of the attractor underlying its dynamics (Fig. 3a). This differentiation is, at the same time, supported by increasing information from the leaf and by elevated generation of new information within the hub itself.

At a coupling strength of $u = 0.1$, the correlation dimension in the hub reaches its maximum value, i.e., $D_2^{(\text{hub})} \approx 4.2$, signaling the establishment of high-dimensional dynamics; by contrast, in the leaves one observes only a minimal increase to $D_2^{(\text{leaves})} \approx 2.3$ (Fig. 3a). The phase coherence $r^{(\text{hub-leaves})} \approx 0.2$ and $r^{(\text{leaves})} < 0.1$ confirms the presence of weak synchronization (Fig. 3b). At this point, the transfer entropy is maximized towards the hub at $T_{X\to Y}/H_Y \approx 0.09$, and considerably larger than in the opposite direction, $T_{Y\to X}/H_X \approx 0.05$ (Fig. 3c). This is accompanied by minimization of information storage in the hub $S_Y/H_Y \approx 0.35$, which becomes markedly lower compared to the leaves, $S_X/H_X \approx 0.45$ (Fig. 3d), and by a correspondingly highest rate of new information generation, $N_Y/H_Y \approx 0.55$ (Fig. 3e). As the couplings are diffusive and undirected, this situation, markedly asymmetric in terms of both the complexity and information flow, arises solely because of the higher node degree distinguishing the hub.

At $u = 0.2$, the correlation dimension remains higher in the hub than the leaves, i.e., $D_2^{(\text{hub})} \approx 3.9$ vs. $D_2^{(\text{leaves})} \approx 2.7$, but the difference is attenuated because the former begins to decay and the latter continues slowly increasing (Fig. 3a). Phase coherence indicates a moderate level of entrainment, with $r^{(\text{hub-leaves})} \approx 0.5$ (Fig. 3b). In the vicinity of this point, the transfer entropies towards the two directions show a crossover, with $T_{X\to Y}, T_{Y\to X} \approx 0.08$ (Fig. 3c). The information stored in the hub begins increasing, i.e., $S_Y/H_Y \approx 0.38$, while that in the leaves remains stable (Fig. 3d), and the rate of new information generation decays in parallel between the two (Fig. 3e). Past this point, the influence that the hub and leaf have on each other continues reversing: stronger coupling brings about rapidly decreasing complexity of the hub dynamics, with a smaller but opposite effect on the leaves.

At $u = 0.3$, one eventually observes similar correlation dimension values between the hub and leaves, i.e., $D_2^{(\text{hub})}, D_2^{(\text{leaves})} \approx 2.9$ (Fig. 3a). At this point, albeit still incomplete, phase synchronization reaches considerable intensity, with $r^{(\text{hub-leaves})} \approx 0.7$ (Fig. 3b). The information flow between the hub and each leaf has become fully reversed, markedly lower towards the former at $T_{X\to Y}/H_Y \approx 0.05$, and about double in the opposite direction, $T_{Y\to X}/H_X \approx 0.1$ (Fig. 3c). The information stored in the hub and leaves becomes similar, i.e., $S_X/H_X, S_Y/H_Y \approx 0.45$ (Fig. 3d), and the rate of new information generation decays further (Fig. 3e).

Second, a vector-driver approach is considered [65], spanning from two leaves to the entirety of the network, with $m = 1, \ldots, n$ to represent the fact that, at a global level, the hub simultaneously interacts with all the leaves. Namely, the time-series of the leaves and hub were described as realizing an $(m+1)$-dimensional network stochastic process $S = \{X, Y\}$, where $X = \{X_1, \ldots, X_m\}$ is the vector process of the m leaves and Y is the scalar process of the hub. Given X_t and Y_t, and considering $X_t^- = [X_{t-1}, X_{t-2} \cdots]$, $Y_t^- = [Y_{t-1}, Y_{t-2} \cdots]$ as the vector variables describing the past of the processes, the information dynamics within the network process S were described and estimated similarly to the above. We denoted the corresponding transfer entropy towards the hub as $\hat{T}^{(m)}_{X\to Y} = I(Y_t; X_t^- | Y_t^-) = H(Y_t|Y_t^-) - H(Y_t|Y_t^-, X_t^-)$. To limit the estimation bias arising from the use of variables having different dimension, all transfer entropies $T^{(m)}_{X\to Y}$, for $m = 1, \ldots, n$ were materially computed considering the full n-dimensional vector process $X = \{X_1, \ldots, X_n\}$ and adopting a distance-projection strategy [67].

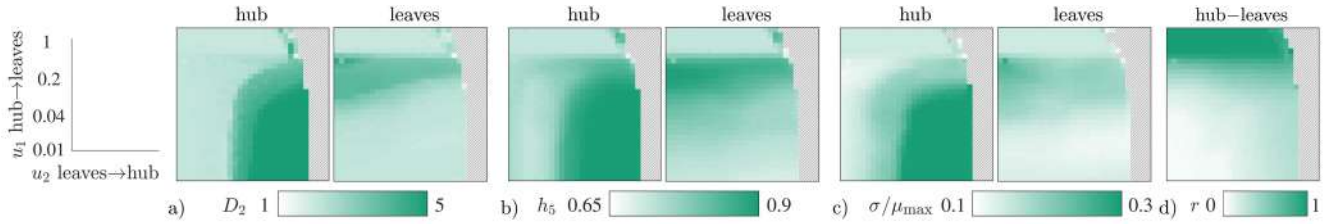

FIGURE 4. Effect of asymmetric coupling strength u_1, u_2 in star networks of Rössler systems with $n = 5$ leaves and $a = 0.35$. a) Correlation dimension D_2 (hub, average of leaves), b) Permutation entropy of adjacent local maxima h_5, c) Coefficient of variation for maxima amplitude fluctuations σ_{max}/μ_{max}, e) Phase synchronization r between the hub and leaves. Hatched areas denote simulation divergence.

This analysis confirms that, at a coupling strength of $u = 0.1$, the information transfer towards the hub monotonically increases the more leaves are taken into account, raising from $\hat{T}^{(1)}_{X\to Y} \approx 0.03$ nat to $\hat{T}^{(5)}_{X\to Y} \approx 0.15$ nat (Fig. 3f). The hub, therefore, on average absorbs information from the entirety of the network as opposed to, for example, preferentially entraining with a subset of one or more leaves as might be expected, for example, in the presence of phenomena such as cluster synchronization [11], [12], [68].

Having established that symmetric couplings may spontaneously give rise to preferential in-flow or out-flow of information between the hub and leaves, the underlying mechanisms can be better elucidated by additionally considering a situation wherein the structural links are made asymmetric by construction. While retaining the same network topology and parameters, we considered, again for $a = 0.35$ and $j = 0, \ldots, n$ the system

$$\begin{cases} \dot{x}_j = -y_j - z_j + \sum_{k=0}^{n} g_{jk}(x_k - x_j) \\ \dot{y}_j = x_j + a y_j, \\ \dot{z}_j = b_j + z_j(x_j - c_j) \end{cases} \tag{10}$$

with the graph

$$g_{jk} = \begin{cases} u_1 & \text{if } k = 0 \wedge j \neq k, \\ u_2 & \text{if } j = 0 \wedge j \neq k, \\ 0 & \text{otherwise} \end{cases} \tag{11}$$

where the coupling coefficients u_1 and u_2 represent, respectively, the outgoing connections towards the leaves (fan-out) and the incoming connections to the hub (fan-in). A 2-dimensional array of settings log-spaced over $u_1, u_2 \in [10^{-2}, 1]$ was simulated.

The interplay between the network topology and the level of link symmetry is readily appreciable. For sufficiently weak coupling towards the leaves u_1, with growing coupling towards the hub u_2 the complexity and irregularity in its dynamics steadily increase, up to $D_2^{(hub)} \approx 6.6$ (Fig. 4a), $h_5^{(hub)} \approx 0.94$ (Fig. 4b) and $\sigma_{max}^{(hub)}/\mu_{max}^{(hub)} \approx 0.54$ (Fig. 4c) before the point past which the simulations diverge. Notably, the phase coherence increases only slightly, up to $r^{(hub\text{-}leaves)} \approx 0.31$ (Fig. 4d), indicating that the hub has a limited possibility of passively synchronizing with the leaves, when it cannot actively attract them towards its trajectory. Assuming that u_2 is sufficiently large to elicit differentiated dynamics in the hub, e.g., $u_2 = 0.1$, one observes an opposite effect of the coupling strength towards the leaves, u_1: as this is increased, the correlation dimension in the hub falls from $D_2^{(hub)} \approx 4.9$ to 2.0 (Fig. 4a), with analogous trends found for $h_5^{(hub)} \approx 0.90$ down to 0.71 (Fig. 4b) and $\sigma_{max}^{(hub)}/\mu_{max}^{(hub)} \approx 0.34$ down to 0.15 (Fig. 4c). The situation, however, is not specular, because increasing the coupling strength towards the leaves markedly raises the phase coherence, up to $r^{(hub\text{-}leaves)} \approx 1$; this is expected, because each leaf is connected to just one hub node and therefore succeeds in synchronizing with it (Fig. 4d).

Considering next the dynamics of the leaves, a different situation is established. The level of dynamical complexity and irregularity remains below the highest values observed for the hub, but there is an intermediate band wherein a transient increase occurs, with a limited effect of the strength of coupling towards the hub u_2. Starting from $D_2^{(leaves)} \approx 2.0$ for sufficiently small strength of the coupling towards the leaves u_1, a gradual elevation is found, up to $D_2^{(leaves)} \approx 4.6$ at $u_1 = 0.1$ (Fig. 4a); analogous effects are observed for $h_5^{(hub)} \approx 0.84$ (Fig. 4b) and $\sigma_{max}^{(leaves)}/\mu_{max}^{(leaves)} \approx 0.22$ (Fig. 4c). Beyond this point, a rapid collapse is found, as the phase coherence increases and the dynamics become undifferentiated with respect to the hub, effectively delineating a master-slave synchronization scenario (Fig. 4d). It is worth noting that the situation is not symmetric in the two directions: for strong coupling only towards the leaves, global synchronization arises and the dynamics become indistinguishable from an isolated Rössler system, whereas, for strong coupling only towards the hub, the trajectories eventually diverge.

In summary, this section sought clarity on the causative mechanisms underlying the non-monotonic effect of the coupling strength visible in Fig. 2. Rigorous information-theoretical accounts are instrumental in attaining an understanding of the interaction patterns arising among coupled chaotic oscillators: these may become highly intricate even in the context of elementary topologies, as exemplified by previous research on the emergence of remote synchronization in ring networks [69]. Furthermore, it is always necessary to confirm any causality inferences based on observation via intervention, in this case, manipulation of the structural

links [30], [64]. These results mainly demonstrate that, even in the presence of undirected couplings, two clearly-distinct regimes emerge as a function of the coupling strength.

At low values, i.e., $u < 0.2$, the hub primarily sinks entropy from the leaves and, as a consequence, stores limited information while generating high-dimensional dynamics. In this region, the collective strength of the links from the leaves towards the hub has a profound impact on its dynamics, but the same does not hold in the other direction, because each leaf only possesses a single connection, therefore the energy (information) exchange rate towards it is considerably lower (1/5, in this case). At high values, i.e., $u > 0.2$, the coupling becomes sufficient to entrain the leaves with the hub; therefore, there is a transient growth in the complexity of their dynamics driven by an outflow of information from the hub, but this is in the context of a general loss of differentiated activity, along the path towards complete synchronization. Such a spontaneous breaking of the symmetry of the identical connections as a function of the global topology appears remarkable.

This account of the dynamics as a function of the coupling strength finds confirmation in the results obtained for asymmetric couplings. These indicated that the dynamics of the hub grow in complexity purely as a function of its ability to receive afferences from the leaves: accordingly, the highest values of the correlation dimension were observed for the most asymmetric, effectively unidirectional, configurations. Such an arrangement resembles a situation wherein the activity from multiple independent dynamical systems is summed, which inherently reflects in a growing fractal dimension of the attractor, up to the point where its geometry becomes statistically indistinguishable from randomness [54]. Here, however, we demonstrated not merely the effect of a sum but the coupling of a dynamical system, and its entrainment in increasingly complex trajectories up to the point of divergence. These results may have practical relevance in wireless networks of electronic oscillators coupled in master-slave mode, such as via radio receivers and transmitters [7]. While additional results are not presented for brevity, we drew analogous conclusions at different settings of the bifurcation parameter a, for non-identical nodes and, as exemplified below, also for structurally-different dynamical systems.

III. COMPLEX NETWORKS OF RÖSSLER SYSTEMS

A. STATISTICAL OBSERVATIONS

While star topologies are instrumental in demonstrating the effect of node degree and are a ubiquitous constituent motif of complex networks, they are seldom observed in isolation within large-scale natural and engineered systems [70]. In this section, we therefore extend the results obtained thus far to encompass two representative types of complex networks, which realize random topologies with or without a scale-free organization, replacing the elementary pattern described by Eq. (2) with a more general unweighted, undirected graph $\mathcal{G}$ representing the couplings among $n = 100$ nodes.

First, we consider the Barabási-Albert model, wherein the graph is constructed through adding nodes one at a time, connecting each new node to $m \leq m_0$ existing ones according to a probability p which increases with the number of their already existing connections. This model thus captures a preferential attachment process of network growth, wherein the most strongly connected nodes attract even more connections, leading to a power-law node degree distribution $P(k) \propto k^{-3}$, which implies the presence of a minority of hub nodes whose degree is disproportionately higher compared to the rest of the network [71]. Here, we set $m_0 = 3$ initially-placed nodes and $m = 2$ number of nodes each new node is connected to, yielding a symmetric network invariably containing 394 links. Second, we consider the Erdős-Rényi model, wherein a graph is constructed through connecting nodes purely randomly, namely, adding each edge with a probability that is independent of all the other edges. As a result, the node degree distribution is binomial and, for sufficiently large and sparse graphs, can be approximated as a Poisson distribution $P(k) \propto (\lambda^k e^{-\lambda})/k!$, where $\lambda = p(n-1)$; in other words, the majority of nodes have the same node degree, with only infrequent deviations, conferring the network a characteristic scale, which contrasts with the inherently scale-free nature of graphs constructed using the Barabási-Albert model [70]. Here, to match the density between the two models, we set $p = 0.04$, yielding a maximally-probable node degree $k = 3$, which is an order of magnitude lower than the degree of the strongest-connected nodes which can be found in the scale-free networks.

Comparing these two models side-by-side in the context of equal density graphs has become commonplace as a means of highlighting the specific effects stemming from scale-free organization [72]. The simulations which follow therefore juxtapose networks having identical size and density, but profoundly different layouts of connections. Even though star motifs can be seen in both models, for the scale-free networks, there is an intuitive appeal in identifying the strongest-connected hub nodes as the core of a restricted population of star topologies, which together strongly determine the cascaded connections across the rest of the network [70].

Retaining the same settings as in Sec. II, 250 random instances of each network type were simulated for every combination of settings for the bifurcation parameter $a \in \{0.25, 0.3, 0.35\}$ and coupling strength $u \in \{0.005, 0.01, 0.02, 0.04, 0.06, 0.08\}$, and average results are presented. All simulation runs were performed using code written in-house and run on a Cray XD1 system (Cray Inc., Seattle, WA, USA).

Some information can be firstly gathered by considering the dynamical measures averaged over the entire network, denoted as $\langle x \rangle$. At the lowest setting of the bifurcation parameter, $a = 0.25$, regardless of the topology, the effect of the coupling strength u is quite limited, with the correlation dimension dwelling around $\langle D_2 \rangle \approx 1.8$ (Fig. 5a), the permutation entropy settling after an initial increase at $\langle h_5 \rangle \approx 0.65$ (Fig. 5b), the coefficient of variation briefly peaking for

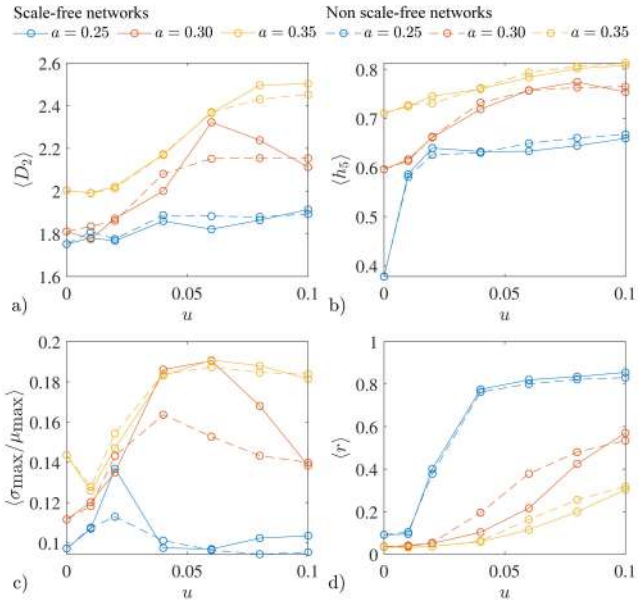

FIGURE 5. Average effect of the coupling strength u and bifurcation parameter a in scale-free (Barabási-Albert model, continuous lines) and non scale-free random (Erdös-Rényi model, dashed lines) undirected networks of $n = 100$ Rössler systems. a) Correlation dimension D_2, b) Permutation entropy of adjacent local maxima h_5, c) Coefficient of variation for maxima fluctuations σ_{max}/μ_{max}, d) Phase synchronization r. Values averaged over runs with different network topologies and all nodes (D_2, h_5 and σ_{max}/μ_{max}) or node pairs (r).

$u = 0.02$ then decaying back to $\sigma_{max}/\mu_{max} \approx 0.1$ (Fig. 5c), and the phase coherence indicating that the system quickly reaches a strongly-synchronized state, with $\langle r \rangle \approx 0.8$ for $u \geq 0.04$ (Fig. 5d). At the intermediate setting of the bifurcation parameter, $a = 0.3$, a noticeable effect of the coupling strength u appears. The correlation dimension increases from $\langle D_2 \rangle \approx 1.8$ to $\langle D_2 \rangle \approx 2.1$ additionally showing, for the scale-free networks only, a non-monotonic trend peaking at $\langle D_2 \rangle \approx 2.3$ (Fig. 5a). The permutation entropy similarly increases from $\langle h_5 \rangle \approx 0.6$ to $\langle h_5 \rangle \approx 0.75$, with closer values between the two networks (Fig. 5b). The coefficient of variation displays a larger and markedly non-monotonic effect, reaching $\sigma_{max}/\mu_{max} \approx 0.16$ at $u = 0.04$ for the non scale-free networks, and the higher level of $\sigma_{max}/\mu_{max} \approx 0.19$ at $u = 0.06$ for the scale-free networks (Fig. 5c). The phase coherence indicates that the system gradually approaches an intermediate level of synchronization, with $\langle r \rangle \approx 0.6$ (Fig. 5d). Finally, at the highest setting of the bifurcation parameter, $a = 0.35$, one observes an even clearer effect of the coupling strength u on the correlation dimension, which increases from $\langle D_2 \rangle \approx 2$ to $\langle D_2 \rangle \approx 2.5$, with similar values between the two network types (Fig. 5a). The change in permutation entropy, though shallower, is concordant, with an increase from $\langle h_5 \rangle \approx 0.71$ to $\langle h_5 \rangle \approx 0.81$ (Fig. 5b). A larger effect is, again, found for the coefficient of variation, which raises from $\sigma_{max}/\mu_{max} \approx 0.13$ to $\sigma_{max}/\mu_{max} \approx 0.18$, with a lessened sensitivity to network topology (Fig. 5c). At this setting, the system reaches at most a state of weak synchronization, hallmarked by phase coherence $\langle r \rangle \leq 0.3$ (Fig. 5d).

Altogether, these results indicate that increasing the coupling strength u between the linked nodes has a global effect on the dynamics, which recalls the observations in the isolated star networks (Fig. 2): namely, growing coupling tends to lead towards higher complexity and irregularity, manifest through elevated correlation dimension, permutation entropy and coefficient of variation. These measures are maximized in a region of weak synchronization, maintaining which requires a sufficiently large setting of the bifurcation parameter a.

To gain further insight, it is necessary to consider local effects reflecting the inherent connectivity heterogeneity, for instance, via binning the nodes according to their node degree k. Taking this perspective, and for brevity initially focusing on the correlation dimension D_2, four key effects emerge, which can be schematized as follows.

First, a marked effect of the node degree k is observed in the scale-free networks, wherein, for suitably large settings of the bifurcation parameter a, $D_2 > 4$ is reached in the most intensely connected nodes (Fig. 6a-c); because their degree distribution is by construction considerably narrower, this effect does cannot emerge in the non scale-free networks (Fig. 6d-f).

Second, in the scale-free networks the effect of node degree k is modulated by both the bifurcation parameter a and the link strength u. At the lowest setting of the bifurcation parameter, $a = 0.25$, the maximum increase is obtained at a coupling strength of $u = 0.01$, peaking at $D_2 \approx 3$ for $k = 36$ (Fig. 6a). At the intermediate setting, $a = 0.3$, the increase becomes more prominent, up to $D_2 \approx 4$ and visible already at lower-degree nodes having $k = 32$; at the same time, at the stronger coupling setting $u = 0.02$, for which no such effect is observed in the previous case, here an even more marked elevation manifests, reaching a plateau $D_2 \approx 4$ for $k \geq 28$, and the gradual increase is already visible at $k = 20$ (Fig. 6b). At the highest setting, $a = 0.35$, a similar pattern is maintained, but translated towards stronger coupling strengths $u = 0.02, 0.04$ and lower node degrees $k \geq 14$ (Fig. 6c).

Third, for practically every setting of the bifurcation parameter a and node degree bin k, a non-monotonic influence of the coupling strength u is found, wherein elevating it the correlation dimension initially increases, then decreases. For example, considering all nodes having an intermediate node degree of $k = 20$, at $a = 0.3$ one observes $D_2 \approx \{1.2, 2.6, 2.3, 1.5\}$ for $u \in \{0.01, 0.02, 0.04, 0.06\}$ (Fig. 6b), and similarly at $a = 0.35$ one observes $D_2 \approx \{2.0, 3.7, 2.6, 1.7\}$ for $u \in \{0.02, 0.04, 0.06, 0.08\}$ (Fig. 6c). The same trend is consistently found for the most intensely connected nodes having $k = 36$, wherein given $a = 0.25$ one observes $D_2 \approx \{1.2, 3.0, 1.4, 1.1\}$ for $u \in \{0.005, 0.01, 0.02, 0.04\}$ (Fig. 6a), and similarly at $a = 0.3$ one observes $D_2 \approx \{4.0, 4.4, 2.8, 1.4\}$ for $u \in \{0.01, 0.02, 0.04, 0.06\}$ (Fig. 6b).

Fourth, for the lowest-degree nodes, e.g. $k \leq 10$, the opposite influence emerges, wherein elevated coupling brings about a decrease in the correlation dimension; albeit less

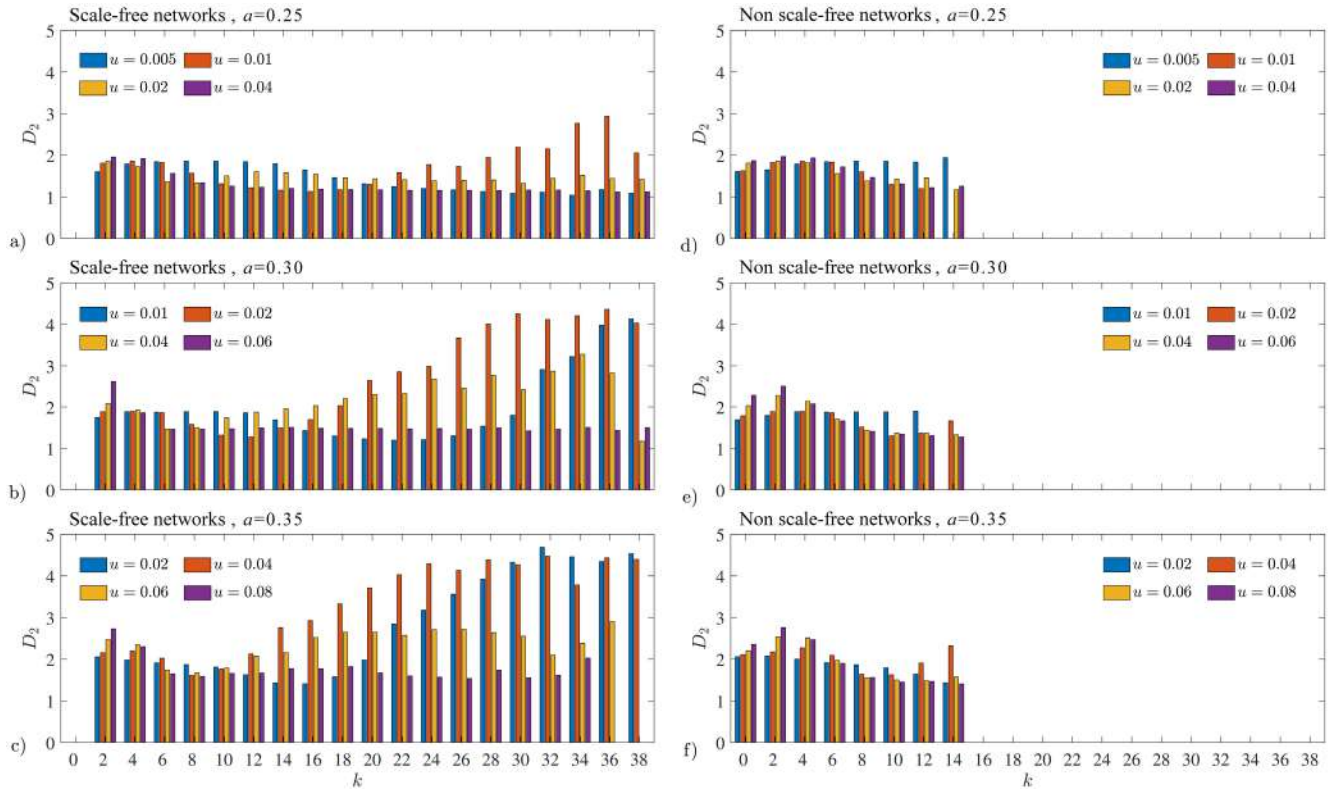

FIGURE 6. Effect of the coupling strength u and bifurcation parameter a as a function of the node degree k (binned as $[k, k+1]$) in scale-free (Barabási-Albert model: a, b and c) and non scale-free random (Erdös-Rényi model; d, e and f) undirected networks of $n = 100$ Rössler systems. Correlation dimension D_2 values for the x variable averaged over runs with different network topologies and all nodes falling into each degree bin.

prominent, this effect is highly consistent. At the lowest setting of the bifurcation parameter, $a = 0.25$, and strongest coupling, $u = 0.04$, in the scale-free networks one observes $D_2 \approx 2$ for $k = 2$ and $D_2 \approx 1.3$ for $k = 10$ (Fig. 6a); because this effect does not require high-degree nodes, it emerges also in the non scale-free networks, wherein one obtains the same values (Fig. 6d). At the highest setting of the bifurcation parameter, $a = 0.35$, the decay becomes even more prominent: in the scale-free networks one observes $D_2 \approx 2.7$ for $k = 2$ and $D_2 \approx 1.7$ for $k = 10$ (Fig. 6c), and in the non scale-free networks one observes $D_2 \approx 2.8$ for $k = 2$ and $D_2 \approx 1.4$ for $k = 10$ (Fig. 6f).

Albeit with some differences, analogous trends are revealed by the other indices, which are therefore not shown for brevity. The sensitivity of the permutation entropy h_5, however, has elements of difference: while at the lowest setting of the bifurcation parameter $a = 0.25$ and intermediate coupling strength $u = 0.01$ one observes a marked increase from $h_5 \approx 0.64$ at $k = 22$ to $h_5 \approx 0.79$ at $k = 36$, at the higher settings of $a = 0.3, 0.35$ a saturation-like effect is rapidly reached, wherein the measure settles around $h_5 \approx 0.9$; on the other hand, permutation entropy seems more sensitive to the effect in the non scale-free networks, showing, given $a = 0.25$ and $u = 0.04$, an increase from $h_5 \approx 0.60$ at $k = 2$ to $h_5 \approx 0.82$ at $k = 14$. Meanwhile, as previously established for the star networks in Sec. II, the coefficient of variation produces results considerably closer to the correlation dimension: for example, given $a = 0.25$ and $u = 0.01$ it increases from $\sigma_{\max}/\mu_{\max} \approx 0.04$ for $k = 10$ up to $\sigma_{\max}/\mu_{\max} \approx 0.42$ for $k = 36$. The non-monotonic effect of coupling strength is also reproduced, for example at $k = 30$, at which $\sigma_{\max}/\mu_{\max} \approx \{0.02, 0.42, 0.19, 0.03\}$ for $u \in \{0.005, 0.01, 0.02, 0.04\}$.

B. ILLUSTRATIVE EXAMPLES

Further insight into the dynamics underlying the differentiation between high- and low-degree nodes is provided by considering a representative example, extracted from a simulation wherein the bifurcation parameter and the coupling strength were initially set to $a = 0.25$ and $u = 0.01$. Visually comparing on a large temporal scale the time-series of activity (x variable of the Rössler system) in a node having degree $k = 31$ (Fig. 7a) with another having degree $k = 3$ (Fig. 7b) reveals that the former is dominated by large and low-frequency cycle amplitude fluctuations, unfolding on a scale approximately one order of magnitude slower than the system intrinsic oscillation period; these are clearly absent for the latter, wherein chaoticity is manifest in the form of faster and less prominent cycle-to-cycle changes. Accordingly, the frequency spectrum for the high-degree node is shifted towards the left, peaking at $f \approx 0.01$, whereas the activity in the low-degree node features a flatter spectrum

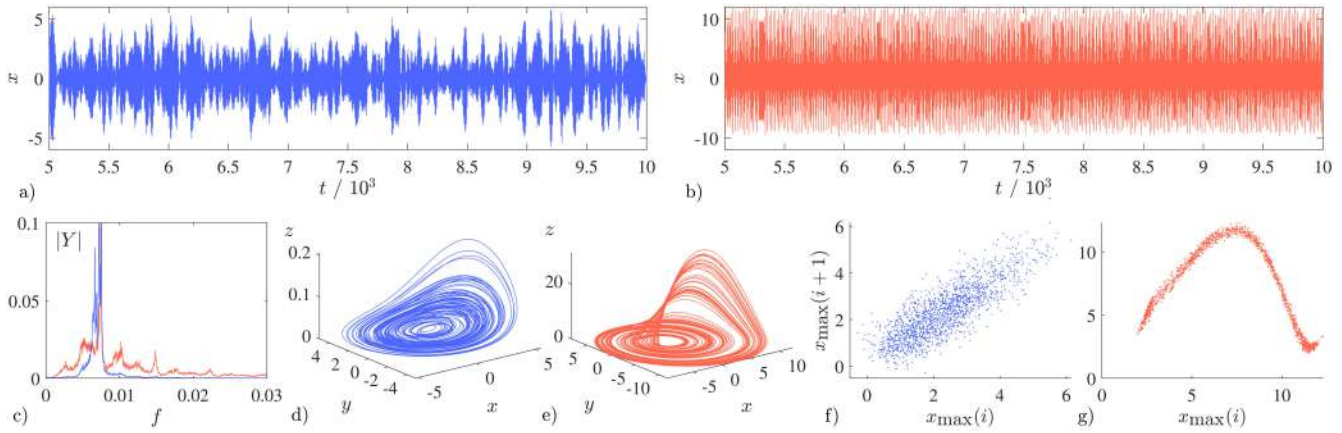

FIGURE 7. Comparison of the dynamics between a high-degree node ($k = 31$, blue) and a low-degree node ($k = 3$, red) in a Barabási-Albert network having coupling strength $u = 0.01$ and bifurcation parameter $a = 0.25$. a) and b) Corresponding time-series, c) Frequency spectra, d) and e) Attractors, f) and g) Poincaré sections from adjacent local maxima. Frequency spectra shown after normalization of signal amplitude to unitary standard deviation and y-axis truncated at 0.1 for comparison.

extending towards higher frequencies (Fig. 7c). An important indication of the underlying mechanism can be obtained by visualizing the phase space in terms of the three system variables. In the high-degree node, the intrinsic dynamics of the system are largely obliterated, because there is no folding and the spikes along the z dimension are reduced to a minimal amplitude: here, irregularity is manifest as fluctuating size of a nearly circular orbit (Fig. 7d). By contrast, in the low-degree node, the folding and spiking characteristic of the Rössler system for the chosen parameter settings are well-evident (Fig. 7e). Even more explicit evidence comes from the Poincaré sections, showing complete dissolution of the map, replaced by a positive correlation between the amplitude of adjacent maxima, for the high-degree node (Fig. 7f) but not the low-degree one (Fig. 7g).

These results fuel important considerations and warnings about the data analysis. First, inspection of the correlation sum slope curves reveals a lack of convergence in the case of the high-degree node; this plausibly stems from the well-known limitations of the estimation method [54], but also points to the need for different approaches to accurately determine the embedding settings in the presence of such kind of multi-scale dynamics [73]. The implication is that the reported values are not quantitatively accurate; instead, they should only be taken as an empirical indicator of a higher level of complexity compared to the low-degree nodes. Second, in the high-degree node, irregularity is manifest as considerably slower amplitude fluctuations compared to the low-degree node. In this study, due to time-series length constraints, we chose an order $m = 5$ for the permutation dimension (representing a typical setting in the literature), making it plausible that the irregular behavior might not adequately be represented in the presence of these slower dynamics, since not enough local maxima are included in the symbol sequence. To remove this concern, additional simulations were run for the example shown in Fig. 7, gathering sufficient data for calculating the permutation dimension up to an order of $m = 8$. Inspection of the corresponding curves shows a complete differentiation between the high-degree and the low-degree node which, furthermore, remains entirely consistent even altering the bifurcation parameter a (Fig. 8a) and the coupling strength u (Fig. 8b); in particular, it is evident that the curves decay more rapidly for the low-degree node, providing clear evidence of lower dynamical complexity. At this point, to allow explicit comparison with the results in Ref. [35], we also calculated the statistical complexity introduced therein and defined as $S_m = h_m Q_m$, where $S_m \in [0, 1]$, h_m is the normalized permutation entropy, and Q_m is a normalized measure of disequilibrium, i.e., distance from an equiprobable distribution. The corresponding trends are different because this index by construction assumes low values when the system appears close to equilibrium, which is the case for low orders m that cannot fully represent the dynamics. Even though the values tend to be lower for the high-degree node, the trend is such that the corresponding values increase faster with m compared to the low-degree node, for which a plateau is reached (Fig. 8c,d). These results underline the importance of model order in these analyses; moreover, we note that, given the absence of any stochasticity in these simulations, the thermodynamical notion of (apparent) equilibrium may not straightforwardly correspond to triviality intended as the absence of structure.

Having established the above, to aid understanding the intricate interplay between node degree k and coupling strength u, it is useful to directly visualize a set of representative scale-free networks, whose dynamics were simulated at the intermediate setting of the bifurcation parameter, $a = 0.3$. For a coupling strength of $u = 0.02$, one clearly observes that the largest-degree nodes, which serve as hubs and as such have a central position in the topology of each network, develop the highest values of correlation dimension (Fig. 9a); in this configuration, the lowest-degree nodes, e.g., $k \leq 5$, show dynamics similar to the uncoupled case, with $D_2 \approx 1.9$, the nodes with intermediate degrees, e.g., $k \in [10, 15]$ exhibit

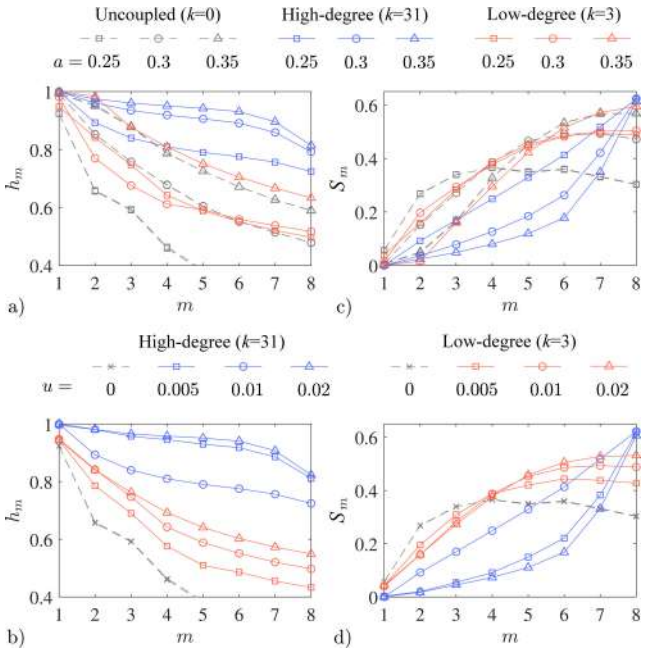

FIGURE 8. Statistical properties of the examples in Fig. 7, for different settings of the model order m. a) and c) Permutation entropy h_m and complexity S_m as a function of the bifurcation parameter a, given a coupling strength of $u = 0.01$, b) and d) Permutation entropy h_m and complexity S_m as a function of the coupling strength u, given bifurcation parameter $a = 0.25$.

a drop down to $D_2 \approx 1.3$, and the small existing fraction of highly-connected nodes, e.g., having $k > 20$, develop up to $D_2 \approx 4.8$. There is, therefore, a non-monotonic effect wherein complex dynamics effectively become "focused" onto the hub nodes, the most peripheral nodes remain largely independent, and the rest of the network follows more ordered dynamics compared to a corresponding ensemble of isolated oscillators. Interestingly, the effect is qualitatively reminiscent of that which iteratively squaring the adjacency matrix has on the nodal strengths [74].

As the coupling strength is increased to $u = 0.04$, the situation begins reversing, and marked heterogeneity is evident, wherein the high-degree nodes are split between those retaining a high correlation dimension and those featuring $D_2 < 2$ (Fig. 9b). At the even stronger coupling setting of $u = 0.06$, the situation has fully reversed, since the largest-degree nodes show the lowest levels of dynamical complexity, and vice versa (Fig. 9c); in this configuration, the most peripheral nodes, with $k = 2$, feature highly-variable values of the correlation dimension, centered around $D_2 \approx 2.8$, which steadily decay with increasing degree until only $D_2 \approx 1.5$ is found for the nodes having a degree of $k > 10$. Notwithstanding their smaller span of node degrees, a similar effect arises in the non scale-free networks, wherein $D_2 \approx 2.5$ for the nodes with $k = 2$, descending to $D_2 < 1.5$ for $k > 8$ (Fig. 9d).

Finally, it is instructive to explicitly consider the interaction between the bifurcation parameter a and the coupling strength u by varying them systematically within one given network. For this purpose, a representative scale-free graph was chosen, and the corresponding dynamical system was simulated 100 times starting from random initial conditions, for each parameter combination obtained while sweeping $a \in [0.15, 0.35]$ and separately setting $u = 0.01, 0.02, \ldots, 0.06$. To better illustrate the relationship between node degree and dynamics, the parametric maps were constructed by sorting the rows in order of descending node degree, namely, $k_i = \{24, 23, 23, 21, 17, 10, 6 \ldots\}$. Considering firstly the correlation dimension D_2, at the lowest coupling strength, $u = 0.01$, there is no effect. Between $u = 0.02$ and $u = 0.05$, a selective elevation of this parameter up to $D_2 > 4$ for the high-degree nodes becomes visible at $a > 0.25$: with increasing coupling, this effect arises then vanishes again. At the strongest coupling strength, $u = 0.06$, the effect is no longer found (Fig. 10a). Albeit with a different pattern, the permutation entropy also reveals a marked differentiation, increasing from $h_5 \approx 0.7$ to $h_5 \approx 0.9$ in the highest-degree nodes, with a graded effect which ensues already at $a > 0.2$ (Fig. 10b). As previously noted, the coefficient of variation follows the correlation dimension more closely, but with sharper edges in this case, jumping from $\sigma_{\max}/\mu_{\max} \approx 0.2$ for $k < 10$ to $\sigma_{\max}/\mu_{\max} \approx 0.40$ for $k > 10$ (Fig. 10c). The sudden change in the latter parameter, and the elevation observed for the correlation dimension, coincided with the transition from strong to weak synchronization, which occurred at increasing values of the bifurcation parameter, namely $a \approx \{0.230, 0.25, 0.27, 0.28, 0.28, 0.29\}$, and earlier in the lesser-connected nodes, delineating an additional effect of node degree (Fig. 10d).

In Sec. II, we primarily focused on how connectivity, symmetric or asymmetric, influences the relationship between a hub and its leaves, revealing a situation wherein increased coupling brings about elevated complexity in the hub, insofar as the coupling strength is not large. Here, those observations were extended to the more naturalistic case of complex networks, highlighting a non-trivial situation wherein the node degree, coupling strength, and bifurcation parameter interact in determining the local dynamics unfolding within each node. On the whole, the results confirm the initial indication that more intense connectivity promotes complexity, insofar as the node degree is sufficiently large and the system is in a weakly synchronized scenario so that a collective behavior does not emerge (Fig. 9a). This assertion finds support in the trends observed for the ensemble values averaged over the entire networks.

Upon closer consideration, however, the relationship is complicated by a plethora of counter-intuitive effects, such as the drop in correlation dimension, which could be elicited in low- and intermediate-degree nodes, while remaining overall far from a situation of strong synchronization (Fig. 9b,c). In other words, it appears that connectivity can both "attract" and "repel" a node from attaining higher complexity, compared to its intrinsic dynamics, as would be observed in an uncoupled arrangement. Our findings recall only in part the observations in Ref. [35], wherein the highest-degree nodes for which we observed an increase were not represented,

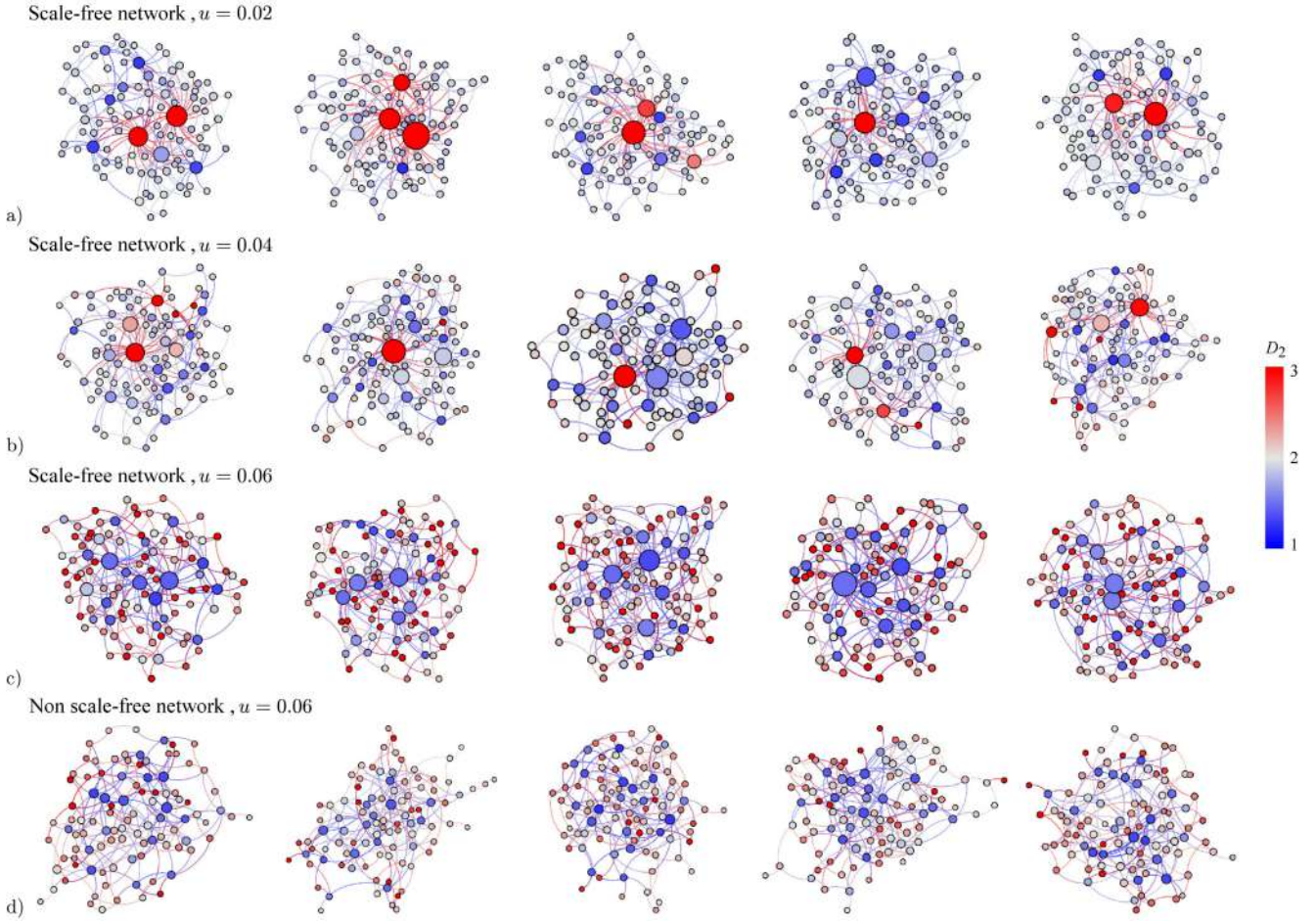

FIGURE 9. Representative examples of the effect of coupling strength u on undirected networks of $n = 100$ Rössler systems having bifurcation parameter $a = 0.3$, for scale-free (Barabási-Albert model: a, b and c for $u = 0.02, 0.04, 0.06$ respectively) and non scale-free random (Erdös-Rényi model; d for $u = 0.06$) topology. Node diameter proportional to degree, and color denotes the correlation dimension D_2 of node dynamics (x variable).

despite the larger network size. More generally, the precise choice of dynamical measure, alongside the practical limitations affecting its practical estimation, appears to play an important role, pointing to the need for more systematic analysis and warning against drawing possibly hasty conclusions regarding general relationships between node degree and dynamics. When considering the temporal dynamics of representative nodes, it could be seen that high connectivity largely obliterates the intrinsic dynamics, replacing them with a highly-irregular overwhelming drive representing the summation of all connected nodes: the geometrical features of the original attractor (as would be observed in the uncoupled system) are washed away but, crucially, the signal is not trivially corresponding to noise, because by construction there are no stochastic dynamics in these simulations.

It was previously shown that scale-free topologies promote the transition to global synchronization between coupled Rössler systems via the effect of loop motifs [75]. Here, in analyzing the path-to-chaos in these networks, we have revealed that the most intensely-connected nodes are those wherein chaoticity becomes primarily, or selectively, manifest as the bifurcation parameter is gradually elevated: based on the results of Sec. II, this appears directly influenced by the node degree. Future work may explicitly evaluate the effect of particular network motifs.

IV. COUPLED ELECTRONIC CHAOTIC OSCILLATORS

A. PHYSICAL REALIZATION

Thus far, numerically-simulated networks of Rössler systems have been considered in this work. Such cases are exemplary because the properties of this low-dimensional system are well-understood, and emergent phenomena are often insensitive to the specific choice of nonlinearity [37], [38]. Nevertheless, to confirm the generality of our findings, in this section a substantially different scenario is investigated, representing another widely-used model of generic nonlinear dynamics.

First, the node dynamics are replaced with the four-dimensional Saito chaos generator [76], which follows

$$\begin{cases} \dot{x}_j = -z_j - w_j + \sum_{k=0}^{n} g_{jk}(x_k - x_j) \\ \dot{y}_j = \gamma_j(2\delta_j y_j + z_j) \\ \dot{z}_j = \rho_j(x_j - y_j), \\ \dot{w}_j = (x_j - h(w_j))/\varepsilon_j \end{cases} \tag{12}$$

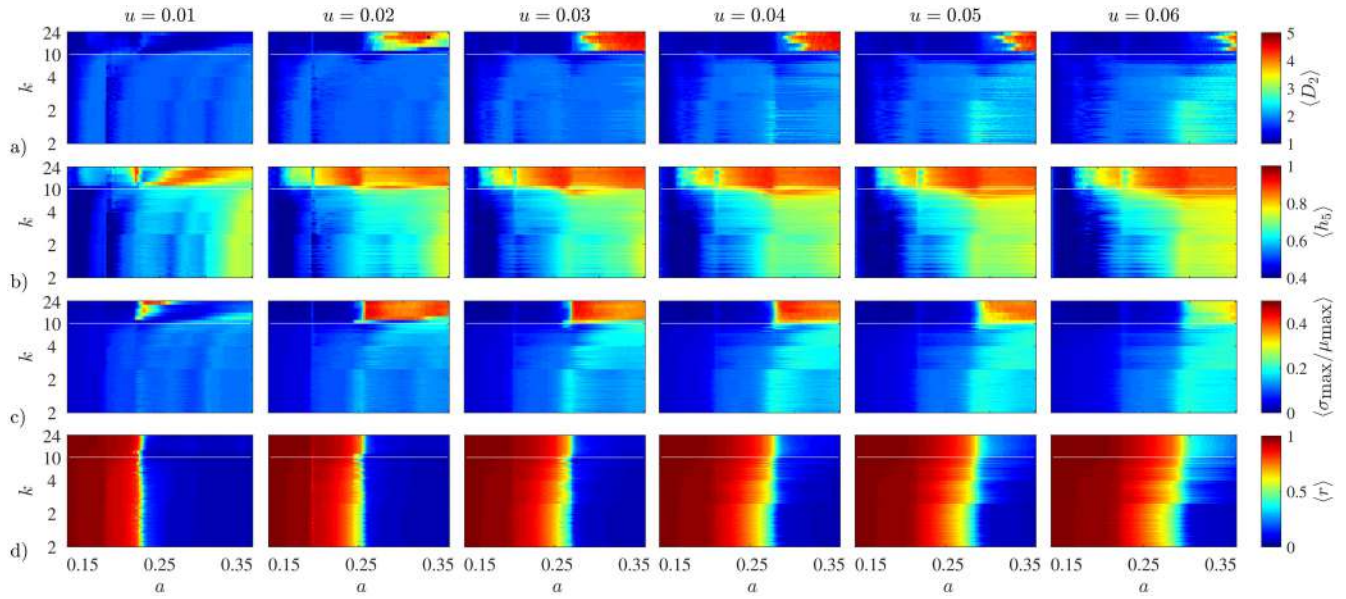

FIGURE 10. Effect of the bifurcation parameter a on node dynamics as a function of degree k and coupling strength u in a chosen representative undirected network of $n = 100$ Rössler systems. For improved visualization, the chart regions corresponding to the most densely-connected nodes (i.e., $k \in [10, 24]$, above white line) have been magnified. a) Correlation dimension D_2, b) Permutation entropy of adjacent local maxima h_5, c) Coefficient of variation for maxima fluctuations $\sigma_{\max}/\mu_{\max}$, d) Average phase synchronization r with the rest of the network. All values averaged over multiple restarts having different initial conditions.

wherein, representing an undirected star graph containing a hub $j = 0$ coupled to n leaves, one has

$$g_{jk} = \begin{cases} u_{jk} & \text{if } (j = 0 \vee k = 0) \wedge j \neq k, \\ 0 & \text{otherwise} \end{cases} \tag{13}$$

and the nonlinearity consists of the piece-wise linear function

$$h(w) = \begin{cases} w - (1 + \eta_j) & \text{if } w \geq \eta_j \\ -\eta_j^{-1} w & \text{if } |w| < \eta_j. \\ w + (1 + \eta_j) & \text{if } w \leq -\eta_j \end{cases} \tag{14}$$

As specified below, an important difference with respect to the cases considered thus far is that here all parameters are subject to small random deviations due to the physical component tolerances, rendering the nodes and link strengths non-identical, i.e., $\gamma_j \approx \gamma$, $\delta_j \approx \delta$, $\varepsilon_j \approx \varepsilon$, $\eta_j \approx \eta$, $\rho_j \approx \rho$ and $u_{jk} = u_{kj} \approx u$.

This system is structurally unrelated to the Rössler equations, in that it comprises three inter-dependent linear equations for $\dot{x}$, $\dot{y}$ and $\dot{z}$, and a separate nonlinear equation for $\dot{w}$, mutually coupled only with the x variable. The time-courses of x, y and z delineate a spiral-like trajectory, whose projection is reminiscent of the behavior of the Rössler system on the x, y plane, whereas the variable w additionally shows sudden jumps, with alternation of high and low values due to the hysteresis effect of $h(w)$. Depending on the control parameters γ, δ, ε, η, and ρ, rich dynamics can be generated, including regions of periodicity, quasi-periodicity, chaos, and hyperchaos. Usually, γ, η and ρ are fixed, $\varepsilon \to 0$ and δ serves as the bifurcation parameter, similarly to a in Eq. (1) [76].

Second, instead of integrating the system numerically, we consider its physical construction in the form of an analog electronic oscillator. This chaos generator was, accordingly, also selected because it lends itself to a compact circuit realization, wherein the function $h(w)$ is approximated by the current-voltage response of two Zener diodes connected anti-parallel in series, and the linear relations are implemented via operational amplifiers [76], [77]. Explicit comparison between simulations and measurements is always fertile because, even when the two should coincide in the asymptotic limit, the dynamics of physical devices are considerably richer due to the presence of more complex relationships, parametric heterogeneities, and non-ideal behaviors [78].

An approximation of this system can be built as shown in Fig. 11a. Given the component values indicated therein, rescaling the amplitudes by $\hat{V} = U_Z r_2/(r_1 + r_2) = 2.55$ V, where $r_2 = r_1 R_1/R_2$, rescaling the time by letting $\dot{x} = \mathrm{d}x/\mathrm{d}\hat{t}$ (and similarly for the other variables), with $\hat{t} = t/\tau$ where $\tau = r_1 C_1 = 39$ μs, then replacing the dynamical variables with $x_j = v_j^{(x)}/\hat{V}$, $y_j = v_j^{(y)}/\hat{V}$, $z_j = r_1 i_j^{(z)}/\hat{V}$ and $w_j = r_1 i_j^{(w)}/\hat{V}$, one has

$$\begin{cases} C_1 \dfrac{\mathrm{d}v_j^{(x)}}{\mathrm{d}t} = -i_j^{(z)} - i_j^{(w)} + \left(v_k^{(x)} - v_j^{(x)}\right)/R_\mathrm{C} \\ C_2 \dfrac{\mathrm{d}v_j^{(y)}}{\mathrm{d}t} = i_j^{(z)} + v_j^{(y)}/R_\mathrm{D} \\ L \dfrac{\mathrm{d}i_j^{(z)}}{\mathrm{d}t} = v_j^{(x)} - v_j^{(y)} \\ L_0 \dfrac{\mathrm{d}i_j^{(w)}}{\mathrm{d}t} = v_j^{(x)} - f(i_j^{(w)}) \end{cases} \tag{15}$$

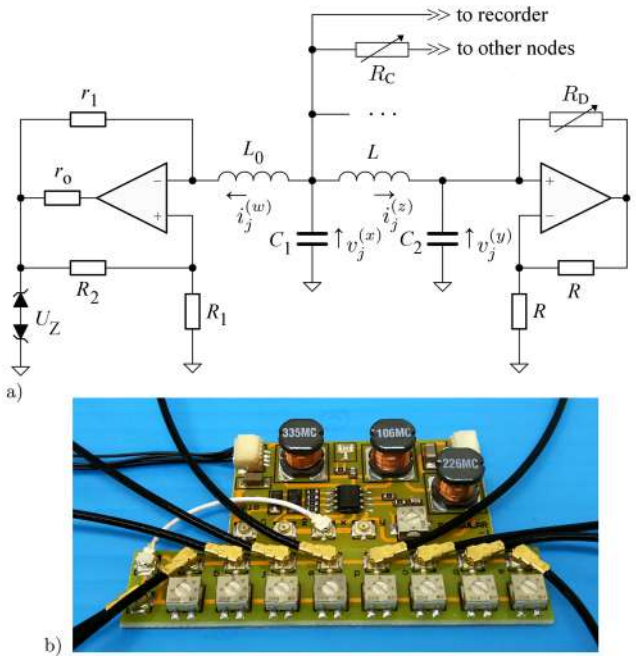

FIGURE 11. Physical realization of the Saito chaos generator. a) Circuit diagram of node j, where the component values are as specified in Table 1; the variable parameters were $R_D \in [5.6, 8.3]$ kΩ and $R_C = \{100, 200, 400\}$ kΩ. b) Circuit boards, implementing the active oscillator (top) and the associated variable coupling resistors (bottom).

and

$$f(i) = \begin{cases} r_1(i - I) - \hat{V} & \text{for } i > I \\ -r_2 i & \text{for } |i| < I, \\ r_1(i + I) + \hat{V} & \text{for } i < -I \end{cases} \tag{16}$$

where $I = \hat{V}/r_2$ [76].

The chosen component values nominally give $\varepsilon = L_0/(r_1^2 C_1) = 0.0085$, $\rho = r_1^2 C_1/L = 12.2$, $\gamma = C_1/C_2 = 1$, and $\eta = r_1/r_2 = 1$; the effect of deviations is detailed in Table 1. The bifurcation parameter was swept by means of the variable resistor R_D over the range $\delta = r_1/(2R_D) \in [0.6, 0.9]$. These settings are close to those for which dynamics of increasing richness were initially observed in Ref. [76], namely, from quasi-periodic for $\delta < 0.78$, to chaotic between $0.78 < \delta < 0.94$, and eventually hyperchaotic for $\delta > 0.94$. However, as loss of oscillatory activity could be observed in this experimental realization for $\delta > 0.9$, the hyperchaotic region was not explored here. In addition, three levels of coupling were evaluated, with $u = r_1/R_C = \{0.025, 0.05, 0.1\}$.

The spontaneous activity was concentrated in the frequency range $f < 30$ kHz, namely considerably below the gain-bandwidth of the operational amplifiers (4 MHz, powered at ±15 V, type TL082; ST Microelectronics S.p.A., Agrate Brianza MI, Italy) and the self-resonances of the inductors (>200 kHz, types 22R335MC, and 22R106MC with 22R226MC in series; MuRata Corp., Tokyo, Japan). However, the realization still represents an approximation of the idealized case, because of $L_0 > 0$ yielding a finite ε, the non-zero current-limiting resistor r_o, and the smooth response of the Zener diodes (type BZT52-C5V1; Nexperia B.V., Nijmegen, The Netherlands). Furthermore, the parametric tolerances were ±10% for L_0, L, C_1 and C_2, ±5% for U_Z, and ±1% for all r and R. The oscillator was realized on a printed circuit board minimizing parasitics, and provided with 8 instances of R_C, allowing coupling to the same number of leaves (Fig. 11b). All links were realized with U.FL-type coaxial cables reducing external interference, and all boards were located > 10 cm apart to avoid spurious inductive interaction between nodes.

TABLE 1. Electronic component values and corresponding derived parameter settings in the Saito chaos generator.

Physical quantities (nominal±tolerance)	Derived parameters (median±95th percentile)
$C_1 = 3.9$ nF ± 390 pF	
$C_2 = 3.9$ nF ± 390 pF	$\gamma = 1 \pm 0.16$
$R = 10$ kΩ ± 100 Ω	
$r_1 = 10$ kΩ ± 100 Ω	
$R_D = 6.25$ kΩ ± 65 Ω†	$\delta = 0.80 \pm 0.012$†
$L_0 = 3.3$ mH ± 330 μH	$\varepsilon = 0.0085 \pm 0.0013$
$R_1 = 10$ kΩ ± 100 Ω	
$R_2 = 10$ kΩ ± 100 Ω	$\eta = 1 \pm 0.016$
$L_0 = 32$ mH ± 3.2 mH	$\rho = 12.2 \pm 1.9$
$R_C = 400$ kΩ ± 4 kΩ†	$u = 0.025 \pm 0.0004$†
$r_o = 820$ Ω ± 8Ω	
$U_Z = 5.1$ V ± 260 mV	

(†): The values of R_D and R_C, and correspondingly the settings of δ and u, correspond to Fig. 12a and Fig. 13b.

When the nodes were electrically uncoupled ($R_C = \infty$) and given a typical setting of the dynamical control parameter ($R_D = 6.25$ kΩ), the frequencies of the largest fluctuations across physical circuit board specimens were $f_j = \{6.174, 6.264, 6.261, 6.262, 6.267, 6.405, 6.395, 5.914, 5.946$ kHz$\}$.

B. EFFECTS OF DEGREE AND COUPLING STRENGTH

Time-series of the voltage $v_j^{(x)}$ were acquired for 5 million points at 1 MSa/s using a recording oscilloscope (type WaveSurfer 3054; LeCroy Inc., Chestnut Ridge NY, USA) connected to a digitally-controlled multiplexer (type MUX508IDR; Texas Instruments Inc., Dallas TX, USA). A representative subset of the dataset has been uploaded to Ref. [79]. The data were analyzed as described in Section II.A, over 20 evenly-spaced segments of 200,000 points each. Because for this system multiple local maxima are contained in each cycle, the map-like representation previously introduced has reduced effectiveness. Therefore, to corroborate the flow-based results obtained with the correlation dimension D_2, we instead resorted to a measure of spectral flatness defined as

$$\xi = \frac{N\left(\prod_{i=1}^{N} a_i\right)^{\frac{1}{N}}}{\sum_{i=1}^{N} a_i}, \tag{17}$$

where N denotes the number of binned Fourier amplitudes a_i [80]. Transition from ordered to chaotic dynamics is universally hallmarked by the generation of a broad spectrum at low frequencies [37], towards which this parameter is

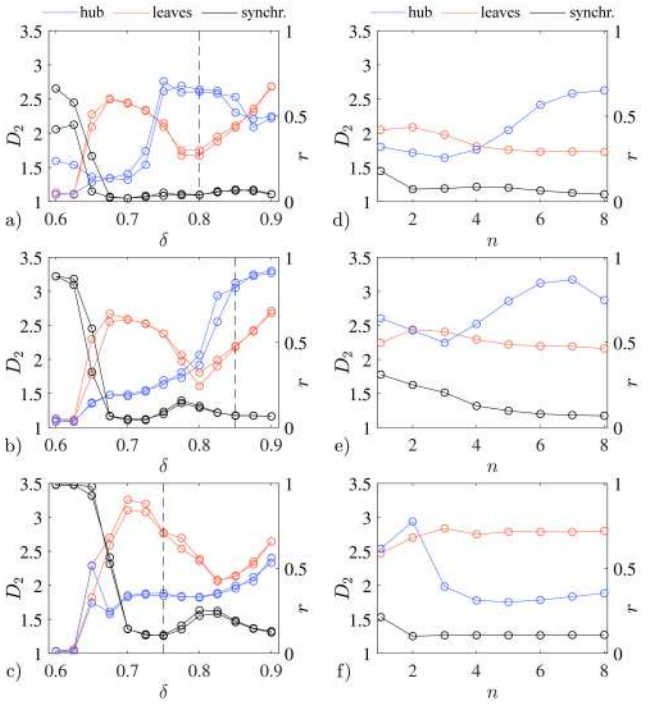

FIGURE 12. Effect of the bifurcation parameter δ and node degree n in the physically-realized star networks of Saito oscillators. a), b) and c) Correlation dimension D_2 (blue: hub, red: average of leaves) and phase synchronization r between the hub and leaves (black) as a function of δ, respectively for $u = 0.025$, 0.05 and 0.1, and $n = 8$. d), e) and f) Correlation dimension D_2 and phase synchronization r as a function of n, respectively for $u = 0.025$ and $\delta = 0.8$, $u = 0.05$ and $\delta = 0.85$, and $u = 0.1$ and $\delta = 0.75$. Duplicated plots reflect realizations instantiating two different physical circuit board specimens at the hub location.

highly sensitive, as also exemplified by previous results on transistor-based chaotic oscillators [81]. Here, it was evaluated over the $f \in (0, 10]$ kHz range.

Considering the full network including $n = 8$ leaves and gradually increasing the bifurcation parameter, for $\delta < 0.65$ one initially observes a region of periodic dynamics in $D_2 \approx 1$, accompanied by significant but incomplete phase coherence $r^{(\text{hub-leaves})} \approx 0.5$ at the weakest coupling level ($u = 0.025$, Fig. 12a), which becomes near-perfect $r^{(\text{hub-leaves})} \approx 1$ at the stronger coupling settings ($u = 0.05$ and 0.1, Fig. 12b, c)

Towards $\delta = 0.7$, the dynamics in the leaves unfold in elevating complexity, peaking at $D_2^{(\text{leaves})} \approx 2.5$ for the two weakest coupling levels (Fig. 12a, b), and reaching a slightly higher value $D_2^{(\text{leaves})} \approx 3.2$ under the strongest coupling condition (Fig. 12c). At this setting of δ, the dynamics in the hub remain considerably less developed, between $D_2^{(\text{hub})} \approx 1.4$ and $D_2^{(\text{hub})} \approx 1.9$ across the weakest and strongest coupling levels. The differentiation of activity is readily appreciable from the underlying signals, which show sustained irregular fluctuations in the leaves alongside a nearly completely periodic oscillation in the hub (Fig. 13a). At this level of δ and those described below, the situation is invariably one of weak synchronization, as indicated by a phase coherence between $r^{(\text{hub-leaves})} < 0.1$ and $r^{(\text{hub-leaves})} \approx 0.15$ (Fig. 12a-c).

Increasing the bifurcation parameter δ further, a crossover is eventually observed, whereby the complexity of the dynamics drops in the leaves but increases in the hub, eventually making the two comparable: this point is found around $\delta \approx 0.74$ at the weakest coupling setting ($u = 0.025$, Fig. 12a), shifts towards the right $\delta \approx 0.78$ at the intermediate setting ($u = 0.05$, Fig. 12b), and cannot be reached at the strongest setting ($u = 0.1$, Fig. 12c). Considering the case of weakest coupling, the dynamics in the hub reach the maximum correlation dimension around $\delta = 0.8$, where one obtains $D_2^{(\text{hub})} \approx 2.6$ in contrast with $D_2^{(\text{leaves})} \approx 1.7$ (Fig. 12a). The differentiation between the hub and leaves is again well-evident upon visual inspection of the underlying signals, which show sustained irregularity in the former and largely periodic activity with only transient turbulence in the latter (Fig. 13b). At the intermediate coupling strength, a similar situation is reached for $\delta = 0.85$, where $D_2^{(\text{hub})} \approx 3.1$ and $D_2^{(\text{leaves})} \approx 2.2$ (Fig. 12b).

Reassuringly, the results are highly consistent with respect to swapping the circuit board at the hub location with another specimen, confirming that they are not consequential to a particular set of component values: this is relevant in the present case, because the physical elements are affected by tolerances, which render the nodes non-identical. Moreover, analogous conclusions are drawn from the spectral flatness. Considering the weakest coupling setting $u = 0.025$, at $\delta = 0.7$, where the correlation dimension peaks in the leaves, one obtains $\xi^{(\text{leaves})} \approx 0.78$ and $\xi^{(\text{hub})} \approx 0.32$. At $\delta = 0.8$, where the correlation dimension instead peaks in the hub, one accordingly gets $\xi^{(\text{hub})} \approx 0.79$ and $\xi^{(\text{leaves})} \approx 0.62$. Here, in the hub the spectrum features two broad components, one extending between 0-10 kHz peaking at ≈ 3.8 kHz, and the other between 10-30 kHz peaking at ≈ 18.9 kHz; by contrast, in the leaves the activity is dominated by a narrow, though not line-like, component at ≈ 5.2 kHz.

To elucidate the effect of network size, selected measurements were repeated for $n = 1, \ldots, 8$ while shuffling the leaves to ensure that they were not influenced by nodes having particular component value combinations. Considering first the weakest-coupling setting $u = 0.025$, and $\delta = 0.8$ at which the hub correlation dimension is highest compared to the leaves (Fig. 12a), two regions are identified. When $n < 4$, $D_2^{(\text{leaves})} > D_2^{(\text{hub})}$, even though the difference is small. At $n = 4$, a crossover is encountered, beyond which the level of complexity rapidly grows in the hub, reaching $D_2^{(\text{hub})} \approx 2.6$ for $n = 8$, while remaining relatively stable for the leaves at $D_2^{(\text{leaves})} \approx 1.7$. It is noteworthy that, in this situation, even though the interaction between hub and leaves is sufficient to sustain a marked differentiation, the phase coherence is effectively zero, i.e., $r^{(\text{hub-leaves})} \approx 0.05$ (Fig. 12d). These observations are confirmed by the spectral flatness, which evaluates to $\xi^{(\text{leaves})} \approx 0.62$ and $\xi^{(\text{hub})} \approx 0.56$ for $n = 1$, $\xi^{(\text{leaves})} \approx 0.63$ and $\xi^{(\text{hub})} \approx 0.67$ for $n = 4$, $\xi^{(\text{leaves})} \approx 0.64$ and $\xi^{(\text{hub})} \approx 0.81$ for $n = 8$.

At the intermediate coupling strength $u = 0.05$, similar trends in n are observed: here, however, the correlation

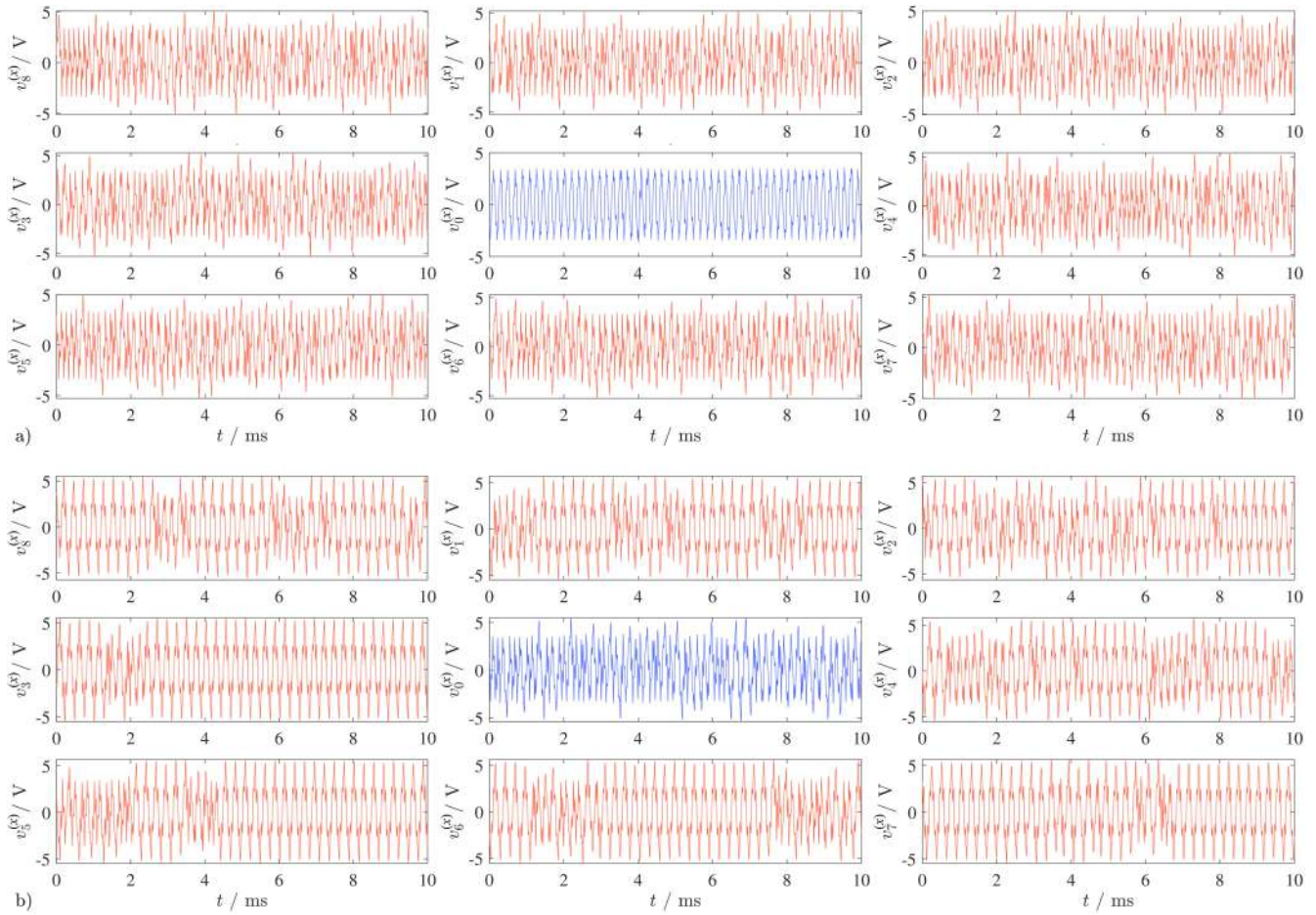

FIGURE 13. Representative experimental time-series of the voltage $v_j^{(x)}$, corresponding to variable x for node j, from star networks of Saito oscillators having $n = 8$ leaves (blue: hub $j = 0$, red: leaves $j = 1, \ldots, n$). a) Recording for $u = 0.1$ and $\delta = 0.75$, b) Recording for $u = 0.025$ and $\delta = 0.8$.

dimension in the hub reaches a higher level, $D_2^{(\text{hub})} \approx 3.2$ at $n = 7$, then drops for $n = 8$; moreover, compared to the previous case, in the leaves a higher $D_2^{(\text{leaves})} \approx 2.2$ is also observed (Fig. 12e).

Finally considering the strongest-coupling scenario $u = 0.1$ at the point $\delta = 0.75$ where the leaves correlation dimension is close to highest with respect to the hub (Fig. 12c), one initially has $D_2^{(\text{leaves})} \approx D_2^{(\text{hub})} \approx 2.5$. For growing network size, a sharp reduction in the correlation dimension is observed for the hub, reaching $D_2^{(\text{hub})} \approx 1.8$ for $n = 4$, whereas in the leaves the dynamics remain relatively unchanged at $D_2^{(\text{leaves})} \approx 2.7$. Attaching more leaves has a negligible effect (Fig. 12f). As before, these results are confirmed by the spectral flatness, which evaluates to $\xi^{(\text{leaves})} \approx \xi^{(\text{hub})} \approx 0.78$ for $n = 1$, $\xi^{(\text{leaves})} \approx 0.80$ and $\xi^{(\text{hub})} \approx 0.44$ for $n = 4$, $\xi^{(\text{leaves})} \approx 0.80$ and $\xi^{(\text{hub})} \approx 0.43$ for $n = 8$.

In summary, these electronic Saito oscillator networks provide results that have aspects of both similarity and difference compared to those reported in the previous sections for Rössler systems. On the one hand, they overall replicate the observations regarding the differentiation of activity between the hub and leaves. In particular, for suitably large settings of the bifurcation parameter, and under conditions of weak coupling, greater complexity spontaneously emerges in the dynamics of the hub, while the leaves dwell in or close to a periodic regime: this recalls Fig. 1 and Fig. 9 for the star and complex networks. Explicit reassurance about the fact that this difference genuinely arises due to the higher node degree of the hub could be gathered by changing the network size (materially disconnecting leaves), thus paralleling the results shown in Fig. 2. For excessively strong coupling, this effect vanishes but the opposite one is found, namely, higher-dimensional dynamics in the leaves compared to the hub, again recalling the results obtained with coupled Rössler systems. On the other hand, at lower-intermediate settings of the bifurcation parameter $\delta \approx 0.7$ the situation appears different, in that higher complexity is consistently detected for the leaves regardless of the coupling strength. In part, these results recall some previous anecdotal observations in coupled Chua's circuits [77].

The non-monotonic influence of the bifurcation parameter, evident particularly for the leaves, deviates from the initial study on an isolated instance of this circuit, wherein elevating δ steadily increased the largest Lyapunov exponent λ_1, eventually also with $\lambda_2 > 0$, plausibly reflecting in a growing

Kaplan-Yorke dimension D_{KY} [37], [76]. This difference is plausibly a reflection of the fact that here a network of coupled units was considered; however, specific aspects related to the present circuit implementation (e.g., L_0-L magnetic coupling within each node) cannot be excluded. The effect of the bifurcation parameter was partially distinct also with respect to the Rössler systems: this may not only be due to the different dynamics, but also stem from the presence of mismatches between nodes in the present case. The latter can play an important role, because the formation of synchronization manifolds between non-identical systems often gives rise to intricate inter-dependencies, which promote or hinder chaotic dynamics across a network or in node subsets [9], [61]. Addressing these issues would require detailed analyses which are beyond the purpose of this work. We note, however, that both patterns of differentiated dynamics between the hub and leaves, especially higher complexity in the hub, were visible in numerical simulations of this system assuming identical or non-identical nodes, which are not shown for brevity. Because in the implemented star network of electronic chaotic oscillators, a situation of different dynamics and presence of mismatches and non-idealities is considered, subject to certain system-specific aspects, the numerical results reported in Sec. II and III appear to have possibly general relevance in physical and natural scenarios.

V. STOCHASTIC SPIKING SYSTEMS

A. SIMULATED NEURONAL MICROCIRCUIT

Thus far, this paper has focused on two systems which are, depending on the numerical or experimental scenario, fully or strongly deterministic. In the physical world, these represent a special case, because non-negligible levels of noise are nearly ubiquitously present. Not only it is knowingly challenging to distinguish noise and chaos, namely structureless versus intricate but deterministic dynamics, but many natural and in particular biological systems are governed by primarily stochastic activity. In other words, while underlying nonlinear dynamics are present, they are largely concealed by random fluctuations, for example of thermal origin [28], [82], [83]. Notably, while in engineered devices noise is often a hindrance to information storage and transmission, self-organized entities such as biological neuronal circuits can leverage it purposefully through phenomena such as stochastic resonance [84]; recently, this effect is also finding applications in nonlinear optics and solid state devices [85], [86]. It is therefore interesting to briefly investigate the influence of local connectivity also in systems with noisy dynamics via the mechanism of stochastic synchronization.

At the same time, particular interest is also attracted by integrate-and-fire activity, namely, excitable entities which store energy up to a threshold then, as consequence of a small fluctuation, release it abruptly in the form of a sudden and discrete event. These systems, which often possess aspects of criticality, are exemplified by action potential generation in neurons, other scenarios including chemical and nuclear chain reactions, crack propagation, phase transition to a low-resistance state in gas discharge tubes [87]–[91]. Their statistical properties can be accurately modeled in the form of point processes, implying that the continuous flow-like evolution of the system variables becomes negligible and the dynamics can be described in a map-like manner purely based on the event timings [28], [92], [93].

Here, we shall therefore investigate the possible effect of connectivity on the emergence of nonlinear structures in time-series of inter-event intervals, first in simulated, then in biological neurons. To this end, we initially consider a model microcircuit, namely, a small-sized neuronal ensemble whose activity is analyzed in terms of all individual spike-trains, thus representing a microscale description. To this end, $n = 7$ spiking cells are represented by instancing the following intrinsically oscillating leaky integrate-and-fire model [94]

$$\dot{v}_j = -v_j + i_j^{(\mathrm{app})} + i_j^{(\mathrm{syn})} \tag{18}$$

where $j = 1, \ldots, n$ and all variables are dimensionless (membrane time constant $\tau = 1$), the synaptic current is an alpha-function

$$i_j^{(\mathrm{syn})} = \sum_{k=1}^{n} g_{jk}\Theta(t - T_k)\alpha^2 e^{-\alpha(t-T_k)}(t - T_k) \tag{19}$$

where $\Theta(x)$ is the Heaviside step function, T_k denote the spike times of neuron k, and each neuron receives an applied current

$$i_j^{(\mathrm{app})} = i_j^{(\mathrm{bias})} + \xi(t) \tag{20}$$

where $i^{(\mathrm{bias})}$ is a homogeneously-applied d.c. term and $\xi(t)$ is a stochastic variable representing a local, independent white noise source, such that $\langle \xi(t) \rangle = 0$ and $\langle \xi(t)\xi(t') \rangle = 2D\delta(t - t')$. Rather than involving the continuous state variables v_j, the couplings are, therefore, realized purely based on the discrete event times T_k.

This network consists of two high-degree neurons $j = 1, 2$ mutually connected via inhibitory synapses to a subset of five low-degree neurons $j = 3, \ldots, 7$. Thus, it can be viewed as the superposition of two stars wherein the separate hubs and shared leaves have, respectively, node degrees 5 and 2 (Fig. 14a); each neuron additionally possesses an excitatory self-synapse. Accordingly,

$$g_{jk} = \begin{cases} w_{\circlearrowleft} & \text{if } j = k \\ w_{\curvearrowleft} & \text{if } (j = 1 \vee j = 2) \wedge j \neq k \\ w_{\curvearrowright} & \text{if } (k = 1 \vee k = 2) \wedge j \neq k, \\ 0 & \text{otherwise} \end{cases} \tag{21}$$

where the weights $w_{\curvearrowleft}$ and $w_{\curvearrowright}$ denote, respectively, the incoming connections to the hubs (fan-in) and the outgoing connections towards the leaves (fan-out), and $w_{\circlearrowleft}$ represents the self-synapse weight. This more complex topology provides an improved opportunity for observing a relationship between connectivity and dynamics, which is expected

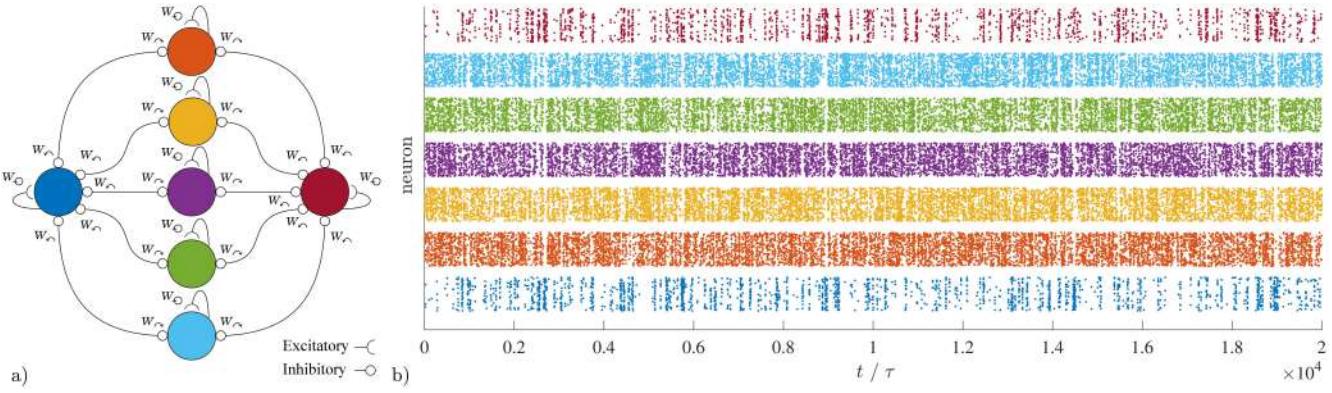

FIGURE 14. Simulated toy model network of leaky integrate-and-fire neurons. a) Network topology, where $w_{\circlearrowleft}$, $w_{\curvearrowright}$ and $w_{\curvearrowright}$ denote, respectively, the self-synapse, fan-out (hub → leaves) and fan-in (leaves → hub) weights; b) Raster plot (τ denotes the membrane time constant). Neurons coded by color, y-coordinate randomly jittered within each band for visualization purposes. Top and bottom bands: hubs, middle bands: leaves.

to be weaker due to the presence of strong stochasticity. Yet, it retains the fundamental characteristic of star graphs, namely, the existence of two node types having a clearly distinct degree. The reciprocal inhibitory synapses between hubs and leaves represent a pervasive motif in the brain, where mutual inhibition, pervasively found for example across hemispheric homologue regions, represents a fundamental mechanism underlying diverse functions from sleep-wake control to decision-making [95], [96]. In this sense, the present network can be considered as a toy model for vastly more complex scenarios. The excitatory self-synapses provide a parsimonious way of promoting self-sustained activity.

For gaging the differences in dynamics between the hubs and leaves, we initially evaluate their average firing rates $f^{(\mathrm{hubs})}$ and $f^{(\mathrm{leaves})}$, together with their Fano factors $F^{(\mathrm{hubs})}$ and $F^{(\mathrm{leaves})}$, which provide a indication of burstiness, namely, propensity to generate over-dispersed event distributions. The latter were calculated binning the point process according to

$$F(T) = \frac{\sigma_T^2}{\mu_T}, \tag{22}$$

where we set bin width to $T = 100$; σ_T^2 and μ_T denote, respectively, variance and mean of the binned event counts.

Because of the expected weak nonlinearity, measures such as the correlation dimension are not appropriate for this system. Instead, we calculated the permutation entropy (Eq. 5), which has superior sensitivity to the presence of ordered structures in the simulated noisy data, and denote it with $h_m^{(\mathrm{sim})}$. Importantly, applying it for the present purpose is more prone to pitfalls compared to the previous sections, wherein it served to measure the complexity of deterministic dynamics. Therefore, rather than considering it directly, we let $h_m^{(\mathrm{surr})}$ represent the permutation entropy of the randomly shuffled time-series and only considered the difference $\Delta h_m = h_m^{(\mathrm{surr})} - h_m^{(\mathrm{sim})}$, for which positive values indicate the presence of structure in the data. This usage stems from recent results demonstrating the successful distinction of chaos and noise based on the systematic comparison to surrogate time-series [97]. We retained the setting $m = 5$, but allowed the lag to span $d = 1, \ldots, 5$ to harvest additional evidence over multiple time scales [57].

We furthermore implemented a simple zeroth-order predictor, which approximates the dynamics locally by a constant. Namely, in delay embedding space, measurements at a time $N + \delta n$ were forecasted by averaging individual predictions based on all neighbors $s_n \in \mathcal{U}_\epsilon(s_N)$ closer than a threshold ϵ, with

$$\hat{s}_{N+\delta n} = \frac{1}{|\mathcal{U}_\epsilon(s_N)|} \sum_{s_n \in \mathcal{U}_\epsilon(s_N)} s_{n+\delta n}, \tag{23}$$

assuming unit delay $\delta t = 1$ and spanning the embedding dimensions $m = 2, 3, 4$. Letting the prediction horizon $\delta n = 1$, the overall prediction error for a measured or simulated signal could be quantified as

$$\varepsilon_m = \sqrt{\langle (s_{n+\delta n} - \hat{s}_{n+\delta n})^2 \rangle_n} / \sigma_s, \tag{24}$$

where σ_s denotes the standard deviation of the data [28]. In this case, all prediction errors were compared with those obtained for surrogate data preserving both the autocorrelation and probability distribution [98]. Denoting with $\varepsilon_m^{(\mathrm{sim})}$ the prediction error from the simulated time-series and $\varepsilon_m^{(\mathrm{surr})}$ the surrogates prediction error averaged over 10 runs, we only considered the difference $\Delta\varepsilon_m = \varepsilon_m^{(\mathrm{surr})} - \varepsilon_m^{(\mathrm{sim})}$, for which positive values again indicate increasing evidence of nonlinear dynamics.

To determine the level of synchronization between each pair of neurons X and Y, we finally calculated the spike cross-correlation function

$$C_{XY}(t) = \frac{1}{\sqrt{N_X N_Y}} \sum_{t_i = t - \delta\tau/2}^{t + \delta\tau/2} X(t_s) Y(t_s - t_i) \tag{25}$$

where t_s indicates the event times the X train, N_X and N_Y represent the number of events in the X and Y trains respectively,

and the bin size was set to $\delta\tau = 1$. From this, the coincidence index (CI) is obtained as

$$\mathrm{CI}_{XY} = \frac{C_{XY}(0)}{\sum_{t=-T}^{T} C_{XY}(t)}, \tag{26}$$

wherein we set the integration span to $T = \pm 100$ [99].

All simulations were run until $t_{\max} = 20 \times 10^3$, for step-size $\mathrm{d}t = 10^{-2}$ and initial conditions $v_j(0) = 0$. Each neuron was deemed to have spiked when $v_j(t) > 1$, and no refractory period was imposed, i.e., $\tau_{\mathrm{refr}} = 0$. The synaptic current scaling, d.c. bias and self-synapse weights were identically set to $\alpha = 4$, $i^{(\mathrm{bias})} = 0.8$ and $w_{\circlearrowleft} = 0.8$ respectively; a noise intensity of $D = 0.02$ was selected (these choices are not critical). A total of $n = 200$ runs were performed for each condition, and average results are presented.

First, we set the weights $w_{\curvearrowleft} = -0.1$ and $w_{\curvearrowright} = -0.15$, realizing a situation wherein the strengths of the individual fan-in and fan-out synapses are on the same order of magnitude: due to their larger node degree, this implies that the two hubs receive an overall stronger inhibitory input. Consequentially, their firing rate $f^{(\mathrm{hubs})} \approx 0.10$ is significantly lower than that of the leaves $f^{(\mathrm{leaves})} \approx 0.47$, and the underlying distributions of inter-event intervals are more right-skewed. Their activity is also markedly more bursty, with $F^{(\mathrm{hubs})} \approx 9.5$ and $F^{(\mathrm{leaves})} \approx 3.8$, as may be appreciated on a raster plot (Fig. 14b). The coincidence index indicates a situation of very weak synchronization: it is largest between the hubs $\mathrm{CI}^{(\mathrm{hubs})} \approx 0.066$, being mediated by inhibition-of-inhibition via the leaves, intermediate among the leaves $\mathrm{CI}^{(\mathrm{leaves})} \approx 0.033$, and smallest between the hubs and leaves $\mathrm{CI}^{(\mathrm{hubs\text{-}leaves})} \approx 0.004$, due to their mutual inhibition. Incidentally, these values are on the same order as those characterizing the biological cultures considered in the next section.

In this configuration, at lag $d = 1$ the permutation entropy difference is positive and larger for the hubs than the leaves, with $\Delta h_5^{(\mathrm{hubs})} \approx 0.0266$ and $\Delta h_5^{(\mathrm{leaves})} \approx 0.0242$; at the longer lags $d = 2, \ldots, 5$ it decreases as expected but the relationship remains unchanged, with $\Delta h_5^{(\mathrm{hubs})} \approx \{0.0144, 0.0076, 0.0042, 0.0026\}$ and $\Delta h_5^{(\mathrm{leaves})} \approx \{0.0115, 0.0053, 0.0025, 0.0013\}$. The prediction error difference provides analogous results across the embedding dimensions, with $\Delta\varepsilon_{2,3,4}^{(\mathrm{hubs})} \approx \{0.0165, 0.0157, 0.0149\}$ and $\Delta\varepsilon_{2,3,4}^{(\mathrm{leaves})} \approx \{0.0150, 0.0146, 0.0133\}$. While quantitatively small, because of their high consistency these effects are statistically strongly significant: two-tailed t-tests always yielded $p < 0.001$, thus demonstrating stronger nonlinear dynamics in the hubs than the leaves.

Second, we set the weights $w_{\curvearrowleft} = -0.025$ and $w_{\curvearrowright} = -0.25$, realizing a different situation wherein there is a less pronounced mismatch between the total strengths of all connections entering each hub and leaf. Consequentially, the difference in firing rates is specular to the previous case, with a significantly higher value in the hubs $f^{(\mathrm{hubs})} \approx 0.49$ than the leaves $f^{(\mathrm{leaves})} \approx 0.13$. The Fano factors are more balanced, namely $F^{(\mathrm{hubs})} \approx 3.3$ and $F^{(\mathrm{leaves})} \approx 4.7$, indicating a similar level of burstiness, lower than observed above for the hubs. The coincidence index also points to a specular situation, because the synchronization is now largest between the leaves $\mathrm{CI}^{(\mathrm{leaves})} \approx 0.070$, smaller between the hubs $\mathrm{CI}^{(\mathrm{hubs})} \approx 0.032$ and smallest between the hubs and leaves $\mathrm{CI}^{(\mathrm{hubs\text{-}leaves})} \approx 0.007$.

In spite of the opposite pattern of firing rate and synchronization, the permutation entropy difference is still larger for the hubs than the leaves, with $\Delta h_5^{(\mathrm{hubs})} \approx 0.0250$ and $\Delta h_5^{(\mathrm{leaves})} \approx 0.0195$; at the longer lags $d = 2, \ldots, 5$ it again decreases as expected but the relationship remains unchanged, with $\Delta h_5^{(\mathrm{hubs})} \approx \{0.0119, 0.0055, 0.0025, 0.0013\}$ and $\Delta h_5^{(\mathrm{leaves})} \approx \{0.0081, 0.0035, 0.0016, 0.0009\}$. As above, the prediction error difference provides analogous results across the embedding dimensions, with $\Delta\varepsilon_{2,3,4}^{(\mathrm{hubs})} \approx \{0.0166, 0.0159, 0.0146\}$ and $\Delta\varepsilon_{2,3,4}^{(\mathrm{leaves})} \approx \{0.0114, 0.0104, 0.0088\}$. All results are significant at $p < 0.001$, confirming that the different dynamics observed for the hub in the first scenario are not merely an artifact due to the firing rate or burstiness, because the differentiation is maintained here even though the differences in these parameters are opposite.

In summary, this simulated toy network of stochastic spiking units extended the results presented in the previous sections, demonstrating an influence of local connectivity in a scenario entirely different from the Rösseler and Saito systems, wherein nonlinearity was strong and couplings were implemented via continuous variables rather than discrete spike events. Here, the higher node degree of the hubs seemingly engendered an elevated expression of deterministic dynamics over a baseline of predominant stochasticity. Remarkably, this effect appeared more closely related to their topological position than the rate distribution of firing activity. While these results should be interpreted cautiously due to greater difficulty in the nonlinear analysis of noisy time-series, they were confirmed by two completely different measures, comparing against two separate surrogate sets (shuffling-based for the permutation entropy, Fourier-based for the zeroth-order predictor). Although further systematic investigations evaluating the effects of the weights together with the noise strength can be carried out, for now it appears noteworthy that, even in this stylized scenario, it was possible to elicit the emergence of more regular and bursty lower-frequency activity in the hubs, contrasted with a higher-rate noise-like activity in the leaves. This observation recalls numerical and analytical results obtained in a star network of biophysically-realistic neurons, wherein it was found that coherent oscillations can arise as a function of the synaptic coupling strength and the network size [100]. Furthermore, a distinction in the same direction was empirically observed in haemodynamic time-series from the human brain acquired at rest, wherein the most densely-connected cortical hub regions generated signals containing stronger signatures of nonlinearity compared to predominantly stochastic activity in the rest of the brain [33]. The present results also appear in line with recent work simulating a larger population of Morris-Lecar neurons instanced over a scale-free topology; in

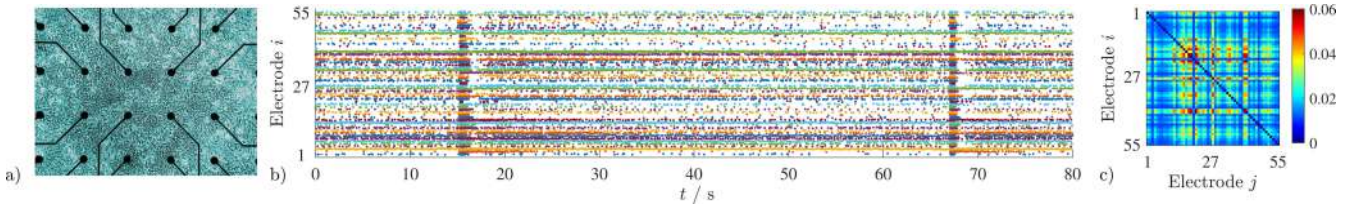

FIGURE 15. Multi-electrode arrays (MEA) recordings of dissociated rat cortical neurons. a) Phase contrast micrograph of a representative culture, courtesy of Dr. D.A. Wagenaar [102]. Electrode pitch: 200 μm. b) Example raster plot showing network bursts. Electrodes coded by color, y-coordinate randomly jittered within each band for visualization purposes and c) Corresponding synchronization matrix (coincidence index CI, within $\Delta t = \pm 10$ ms).

that context, weak coupling elevated the statistical complexity S of firing in the hub neurons, indexing a deviation from purely noise-like dynamics [35]. While a detailed comparison is beyond scope, we report that the same measure revealed an analogous effect in the first configuration considered here, yielding $S_5^{(\text{hubs})} \approx 0.13$ and $S_5^{(\text{leaves})} \approx 0.07$.

B. DISSOCIATED NEURONAL CULTURES

Finally, we demonstrate that the results obtained simulating the stylized neuronal microcircuit generalize to a vastly more complex case, consisting of in-vitro neuronal cultures. Namely, the spontaneous firing activity was recorded from biological cortical neurons, which were harvested from rat embryos, mechanically dissociated to destroy the bulk of initial connections, then plated on glass culture wells containing multi-electrode arrays (MEA) [101]. Besides the biological vs. numerical nature of the experiment, this dataset is different in that it represents a mesoscale scenario, because each culture is obtained by plating $\approx$ 50, 000 cells in a droplet covering an area with $\approx$ 5 mm diameter, instrumented by an array of 8×8 electrodes having 200 μm pitch: each channel, therefore, captures the ensemble activity of $\approx$ 100-1, 000 neurons (Fig. 15a). In a suitable medium, the dissociated neurons spontaneously regrow new axonal connections over a range of up to a few millimeters, forming a pattern that is entirely self-organized and, as such, translates into highly variable, yet consistently rich, activity [102]. After plating, these cultures are initially immature and, therefore, nearly electrically quiescent or generating spikes that are spatially uncorrelated. Such activity becomes increasingly visible after $\approx$ 10 days in-vitro (DIV) and develops until $\approx$ 30 DIV, past which neuronal death ensues and the cultures gradually degenerate. The data were drawn from a public repository, available at Refs. [102], [103], wherein the experimental methods including signal filtering and spike detection are detailed.

The high density of overlapping neurites renders it presently not possible to map the synaptic layout without recourse to techniques that require fixation and are therefore destructive, such as confocal microscopy. As a proxy of structural connectivity, then, in this section functional connectivity is considered for comparison with the dynamics. The association between the two is knowingly maximized when the analysis is restricted to network bursts, that is, sporadic events during which synchronicity extends to a considerable fraction of the culture, or even the totality of it (Fig. 15b) [99]. Here, these were segmented by first identifying bursts at the level of single electrodes in terms of temporal clustering (minimum inter-spike interval $\approx$ 0.1 s, adaptively set), then retaining only the time-intervals wherein simultaneous bursting involved $>$ 5 electrodes. On the remaining spikes, connectivity was thereafter estimated via the coincidence index (CI, Eq. 27), setting a window size of $\delta t = 10$ ms (comparable results can be obtained with $\delta t = 25$ ms); while index choice remains a contentious matter, additional analyses not shown for brevity confirm the results based on alternative assumptions, including approaches involving smoothing the point-processes to recover and correlate continuous time-series [104]. In this scenario, node degree and synaptic strength are not accessible. Therefore the level of connectedness of each node is represented through its nodal strength, empirically defined as

$$w_j = \sum_{j=1, j \neq k}^{n} \text{CI}_{jk}, \tag{27}$$

where the network size n is defined as the number of active electrodes, namely, those for which at least one burst and 64 spikes are obtained. This approach is justified by the fact that the cultures develop inhomogeneous activity, such that some nodes are noticeably more synchronized than the others, conferring to the corresponding matrices a characteristic ''striped'' appearance (Fig. 15c) [74]. As in the simulated microcircuit, the coincidence levels observed, namely up to CI ≈ 0.06, are indicative of operation in a weak synchronization regime, which represents a pervasive requirement for the maintenance of healthy neuronal dynamics [18].

In line with previous observations, the network size n increases with age, from $n \approx 34$ at DIV 10 up to $n \approx 49$ at DIV 24, then begins to decline (Fig. 16a); correspondingly, the average firing rate raises from $f \approx 2$ Hz at DIV 10 up to $f \approx 6$ Hz at DIV 24 and 31 (Fig. 16b). This trend of steady development followed by incipient degeneration is even more clearly evident in terms of the Fano factor ($T = 10$ ms, not critical), raising from $F \approx 1.2$ at DIV 10 to $F \approx 2.2$ at DIV 24 (Fig. 16c), and of the nodal strength, raising from $w \approx 0.8$ at DIV 10 to $w \approx 3.3$ at DIV 24 (Fig. 16d); for DIV 31, F and w are both slightly lower. In the first scenario of the simulated microcircuit, in the two hubs the firing rate was lower and the burstiness was higher compared to the leaves: notably, the same associations are found here between recording electrodes, in terms of the rank-order correlations between the firing rate and nodal strength $\rho[f, w] \approx$

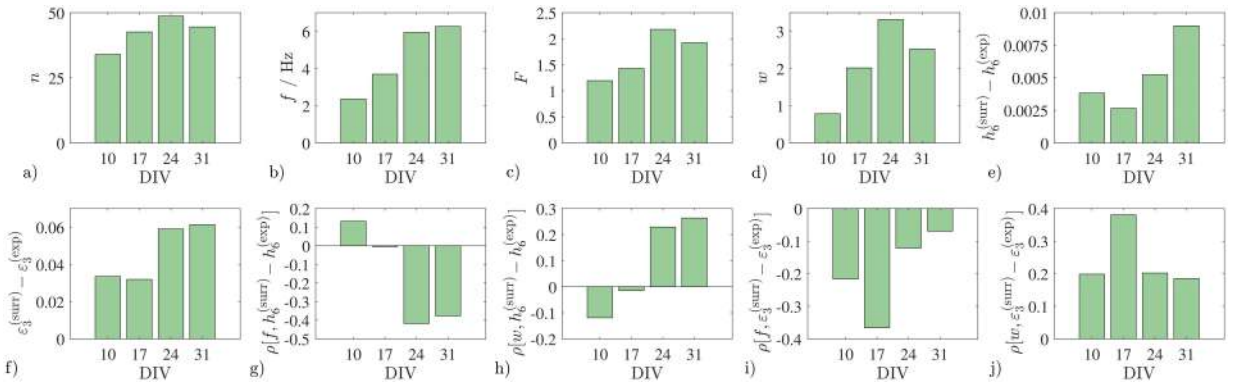

FIGURE 16. Statistical properties of neuronal activity as function of culture age (days in-vitro, DIV 10, 17, 24 and 31). a) Number of active electrodes n (culture size), b) Average firing rate f, c) Fano factor F, d) Weighted nodal strength w, e) Permutation entropy difference between the surrogate and experimental spike trains $h_6^{(\mathrm{surr})} - h_6^{(\mathrm{exp})}$, f) Prediction error difference between the surrogate and measured spike trains $\varepsilon_3^{(\mathrm{surr})} - \varepsilon_3^{(\mathrm{exp})}$, g)-j) Rank-order correlation coefficients $\rho[x, y]$ between these parameters.

$\{-0.49, -0.76, -0.72, -0.69\}$, and between the Fano factor and nodal strength $\rho[F, w] \approx \{0.22, 0.35, 0.07, 0.06\}$, averaged separately over DIV 10, 17, 24 and 31.

To highlight the correspondence between the two scenarios, the same nonlinear approaches as in the previous section are used: importantly, to this end all spike events were considered, without performing any kind of burst filtering, which would inherently corrupt the dynamics. Considering firstly the permutation entropy difference with respect to the shuffled surrogates, $\Delta h_6 = h_6^{(\mathrm{surr})} - h_6^{(\mathrm{exp})}$, for lag $d = 1$ one observed a steady increase, from $\Delta h_6 \approx 0.0038$ at DIV 10 to $\Delta h_6 \approx 0.0090$ at DIV 31 (Fig. 16e); the effect persists and becomes even stronger for longer lags, for example at $d = 5$ one has $\Delta h_6 \approx 0.0039$ at DIV 10 and $\Delta h_6 \approx 0.0228$ at DIV 31. Here, $m = 6$ was chosen given as the highest value at which the median spike-train length exceeds $5m!$. Considering next the prediction error difference with respect to Fourier amplitude- and value distribution-preserving surrogates, $\Delta\varepsilon_3 = \varepsilon_3^{(\mathrm{surr})} - \varepsilon_3^{(\mathrm{exp})}$, one similarly observes a lower level $\Delta\varepsilon_3 \approx 0.032$ at DIV 10 and 17, and a higher level $\Delta\varepsilon_3 \approx 0.060$ at DIV 24 and 31 (Fig. 16f); also in this case, the embedding dimension had limited effect, i.e., $\Delta\varepsilon_{2,4} \approx \Delta\varepsilon_3$. Notably, both the permutation entropy and nonlinear predictor show that the dynamics of spontaneous activity are markedly more structured at the latter time-points compared to the first two.

While such age-related effects are notable, greater interest lies in the relationship between these indicators of nonlinear dynamics and the other features which distinguished the hub nodes in the simulated microcircuit considered previously. The permutation entropy difference shows a negative correlation with firing rate that depends markedly on culture age: across DIV 10, 17, 24 and 31, for $d = 1$ one has $\rho[f, \Delta h_6] \approx \{0.12, 0.00, -0.41, -0.39\}$ (Fig. 16g). At the age when the effect is most marked, namely DIV 24, changing the lag confirms the robust association, with $\rho[f, w] \approx \{-0.60, -0.54, -0.41, -0.31\}$ given $d = 2, \ldots, 5$. Concerning the effect of nodal strength, the hypothesized specular relationship is well-evident: across DIV 10, 17, 24 and 31, for $d = 1$ one has $\rho[w, \Delta h_6] \approx \{-0.11, -0.04, 0.22, 0.26\}$ (Fig. 16h). Also in this case, probing longer time-scales via increasing the time lag d confirms the initial finding; in fact, for $d = 3$ even stronger correlations are revealed, with $\rho[w, \Delta h_6] \approx \{0.15, 0.45, 0.39, 0.30\}$. Such differentiation, wherein signatures of nonlinear dynamics emerge preferentially for nodes that fire at a lower frequency and have higher synchronization, then emerges as a product of the maturation process in these biological preparations.

Albeit with some differences, analogous conclusions are drawn based on the nonlinear prediction error. Its difference with respect to surrogates is always negative: across DIV 10, 17, 24 and 31, for $m = 3$ one has $\rho[f, \Delta\varepsilon_3] \approx \{-0.22, -0.37, -0.12, -0.07\}$ (Fig. 16i). Here, the age at which is effect is strongest is a week earlier, namely DIV 17; at this point, one has $\Delta\varepsilon_{2,3,4} \approx \{-0.43, -0.37, -0.27\}$. Again, the effect of nodal strength is found in terms of a nearly-specular pattern: across DIV 10, 17, 24 and 31, for $m = 3$ one has $\rho[f, \Delta\varepsilon_3] \approx \{0.20, 0.38, 0.20, 0.19\}$ (Fig. 16j). At DIV 17, changing the embedding dimension one observes $\Delta\varepsilon_{2,3,4} \approx \{0.45, 0.38, 0.31\}$. In other words, the permutation entropy and prediction error provide convergent indications regarding the relationship between nonlinear dynamics, nodal strength and frequency; however, their sensitivity appears to differ, in that the former finds the strongest associations at DIV 24, and the latter at DIV 17.

Omitting for brevity a detailed comparison, we note that application of the measure of statistical complexity introduced in Ref. [35] provides comparable results. On the one hand, across DIV 10, 17, 24 and 31, the average complexity appears to decrease, with $S_6 \approx \{0.35, 0.28, 0.22, 0.21\}$, and the correlation with firing rate is nearly invariably complete, with $\rho[f, S_6] \approx -1$. On the other, the correlation with nodal strength is positive and increases with culture age, peaking at DIV 17 as observed for the nonlinear prediction error, with $\rho[w, S_6] \approx \{0.48, 0.74, 0.70, 0.65\}$.

Having thus far considered the effects at a statistical level, it is instructive to visualize a selection of 6 arbitrarily-chosen but representative cases, for which the difference in nonlinear prediction error is compared with the connectivity strength. Although substantial variability is always evident, one notes

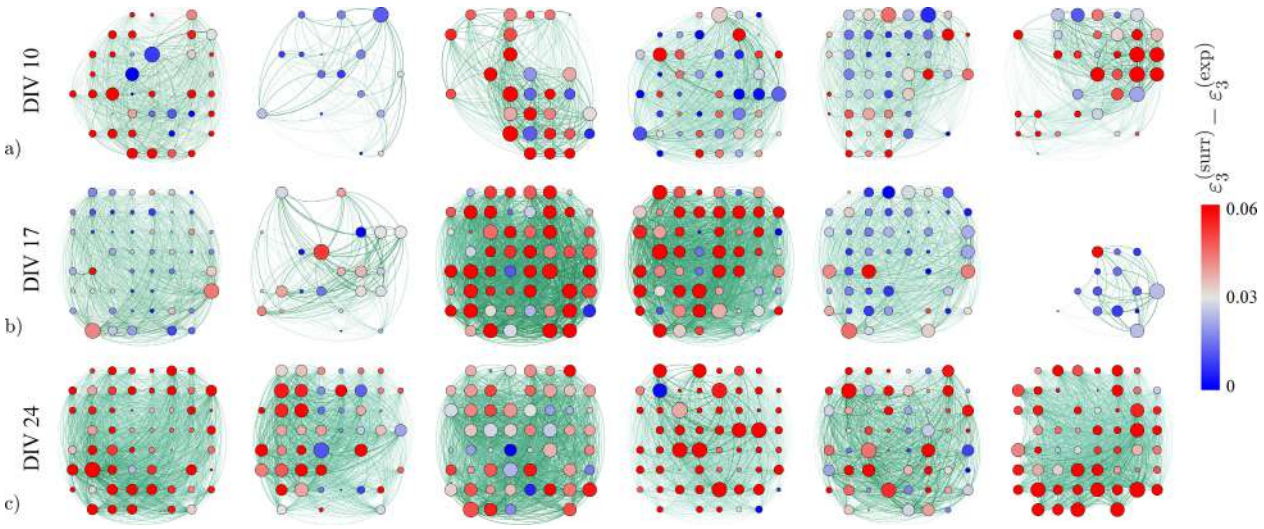

FIGURE 17. Synchronization networks formed by representative neuronal cultures of different age, namely a) days in-vitro (DIV) 10, b) DIV 17 and c) DIV 24. Green intensity denotes edge strength (synchronization level), node diameter proportional to weighted nodal strength, node layout reflects electrode locations, and node color denotes the prediction error difference between surrogate and measured spike trains $\varepsilon_3^{(surr)} - \varepsilon_3^{(exp)}$.

that at DIV 10 the network density (synchronization level) remains on average low, and the prediction error differences accordingly also remain low; for some networks, there are, however, a minority of strongly-connected nodes (large diameter), and these tend to be associated with a positive prediction error difference (red hue; Fig. 17a). One week later, at DIV 17, the prediction error difference is unchanged in some cultures, but reaches considerably high levels in others, which are found predominantly in the most densely-connected nodes (Fig. 17b). At DIV 24, the networks appear even further developed: consequentially, the prediction error difference is more pervasively positive, therefore less associated with nodal strength (Fig. 17c).

While the simulated microcircuit considered in the previous section represents a stylized motif, these living cultures possess a vastly more complex architecture, in a sense paralleling the difference between the star and complex networks of Rössler oscillators considered in Sec. II and III. In this case, however, a profound difference in scale is also present, on the order of 3-4 orders of magnitude, affecting not only the system size but also the granularity at which the activity is represented in each point process. It, therefore, appears remarkable that convergent results were obtained, indicating that the emergence of a nonlinear structure is associated with nodes that fire more infrequently but in a more synchronized manner, additionally showing slow fluctuations in terms of bursts. The spontaneous evolution of these cultures represents a highly individualized interplay of a multiplicity of factors including homeostasis and preferential attachment [102], which eventually lead towards an organization which is small-word and scale-free [105], and geared towards the collective operation close to criticality [106]. In this sense, such preparations can be viewed as a mesoscale equivalent of the features of entire brains, which are typically studied at an even coarser spatiotemporal resolution [78].

It should not be surprising, then, that these results also map closely onto those previously reported for hemodynamic time-series, which also delineated a close association between node degree of synchronization and the convergence of correlation dimension estimation taken as a proxy of nonlinearity [33]. Notably, a correspondence between the in-vivo and in-vitro scenarios was also discussed in a previous study, wherein it was found that signatures of chaotic dynamics gradually ensue in these cultures, as a function of age and culture size [107]: the present results are in line with that report, but crucially add the explanatory factor of connectivity intensity (nodal strength) as a determinant of spatial (topographical) differences in the generation of nonlinear dynamics over a background of stochastic activity. The notion that higher synchronization, stemming from stronger coupling, leads to more structured dynamics also rhymes with the idea that mutual entrainment may be a way for neuronal ensembles to protect themselves from unavoidable noise sources (e.g., thermal noise), thus making it possible to purposefully generate coherent signals [108].

VI. CONCLUDING REMARKS AND POSSIBLE APPLICATIONS

This multidisciplinary study addressed the as-yet relatively under-investigated but fundamental topic of the effect that connectivity has on the local dynamics unfolding within each node in a generic natural or artificial network. Firstly, the elementary case of star topologies was considered, and it was shown via simulations of Rössler systems that increased coupling favors the development of complex dynamics, insofar as the links are not so strong as to move away from the regime of weak synchronization and cause the system to start developing a collective behavior. Through information-theoretical analyses, it was illustrated that elevated complexity in the hub could be driven by information inflow from the leaves, a conclusion that was also supported by simulations with asymmetric couplings. Second, scale-free and non scale-free

graphs were investigated, and similar conclusions were drawn; besides differences directly stemming from their node degree distributions, some additional effects not evident in the star networks were found. In particular, the possibly non-monotonic influence of connectivity was more clearly revealed, wherein, depending on the coupling strength, elevated levels of complexity could be observed in the highest or lowest degree nodes. Third, the results were extended to an experimental scenario, namely a star network of electronic chaotic oscillators. Given the situation of different dynamics and presence of mismatches and non-idealities, this confirmed the possibly general relevance of the numerical results, in particular, the effects of node degree and coupling strength. Fourth, a stochastic spiking system representing a neuronal microcircuit was simulated, and it was found that in such a context, elevated connectivity can lead to the emergence of stronger signatures of nonlinearity, established over a baseline of noise-like activity. Finally, similar conclusions were drawn based on experimental data from biological neuronal cultures on multi-electrode arrays.

In summary, this work indicates that relationships between the local connectivity of each node and its dynamics can arise across rather diverse scenarios. The specific trend, however, seems to depend on a multitude of features, including the topology of the entire network. As such, our results corroborate and extend recent work in this direction, also cautioning against assuming that a simple relationship holds universally [35], [62], [63]. Interestingly, the effect of connectivity was, at least on the surface, effectively diametrically opposite in scenarios of strong and weak determinism of the elemental dynamics. In the former case, elevated couplings lead to more complex activity in the hub nodes, thereby rendering the presence of deterministic relationships more difficult to detect. Taking human interactions as a metaphor, this recalls the common experience that people with a high number of social connections, such as managers, tend to have considerably more erratic and unpredictable schedules than other employees [109]. On other hand, in the latter case, the effect was to attenuate the noise and thus render activity more ordered and predictable.

Another relevant aspect of this work is the systematic comparison of different measures of complexity and nonlinearity, primarily the correlation dimension, permutation entropy and prediction error, which led to convergent but not fully overlapping results, thus highlighting the importance of further addressing the effect of measure choice in this area. Given the intricate nature of the effects, the fundamental relationship between local connectivity and dynamics should be more extensively addressed in the future, to better elucidate the multiplicity of factors which determine it, including possibly system-specific aspects.

Although this topic has as-yet received limited attention compared to the effect of connectivity on synchronization, the potential implications of a more detailed understanding of the relationship between connectivity and local node dynamics are manifold [11]–[13], [68], [75]. As engineering inexorably transitions towards a focus on highly distributed systems, with ever finer granularity, it will become essential to understand how weakly- and strongly-connected nodes can behave differently. For example, in digital relay networks, as encountered in IoT contexts, some nodes may, in virtue of their location, be more likely to interact, namely exchange data or synchronize, with a large number of neighbors [4], [5]. One particular instance of interest is the realization of distributed sensing systems operating via wirelessly-coupled nonlinear oscillators, such as transistor oscillators [110], [111]. Such entities can be used to sense a broad range of physical variables unintrusively, such as soil nutrient content, and their behavior and the variable of interest for data acquisition is a distributed information based both on the locally sensed quantity and the knowledge of this variable at neighboring, linked sites. As coupling strengths may depend on distance, the present results suggest that the homogeneity of the topographical distribution of nodes can have a profound effect. Namely, sparsely-distributed networks with regions of high-density are predicted to be more likely to generate high-complexity, possibly chaotic, behaviors compared to dense and more homogeneous networks, where a more ordered and highly-synchronized collective state is likely to emerge. In these contexts, there may be situations wherein high- or low-complexity activity is desirable. When dynamics are primarily stochastic, for example, due to the overlap of noise-like transactions from unrelated end-points, according to the present results creating highly-coupled nodes could be a way to engender the emergence of more predictable network activity; this might have relevance to the control of power distribution and telecommunication networks [6], [7]. These speculative assertions will be evaluated in future applied research.

The analysis of the complexity at the level of individual nodes presented may herein be of interest also for network identification and control. At a general level, it may contribute to the detection of emergent properties and identification of the vital nodes which influence and sustain the network dynamics [8], [21], [22]. In network control, given the high number of elements of the system, it is difficult or even impossible to apply an action to each node and, for this reason, several efforts have been devoted to understanding which sites enable the full [112] or partial [113] control of the network. Our conclusions in some aspects complement these results that are mainly focused on the linear nodal dynamics case. In the case of isolated dynamics, the control of chaos has led to many techniques either aiming at suppressing or promoting a chaotic behavior [114]. The results of our study can provide directions to extend these techniques to networked systems as, on the one hand, they may inform the selection of the units to pin for control by identifying the nodes having the highest or lowest level of complexity and, the other hand, they may unveil the mechanisms underlying the differentiation of the complexity at the node level and, therefore, promote a better understanding on how to control this differentiation.

Finally, these results are relevant to the interpretation of neurophysiological time-series. In a previous study, it was shown that the hub regions of the cortex generate signals which large-amplitude, low-frequency fluctuations which contain stronger signatures of nonlinearity compared to the rest of the brain, wherein, under resting conditions, the activity appears mostly as noise-like higher-frequency fluctuations [33]. Here, such observation was extended to neuronal cultures and a simulated microcircuit. The present results reinforce the connection to several simulation studies, wherein it was shown that connectivity could lead to the emergence of the low-frequency coherent fluctuations which are tracked by hemodynamics and, therefore, visible to techniques such as functional MRI [115]. More generally, because it seems possible to establish a relationship between the connectivity of each network node and its dynamics, this work motivates more extensively investigating such a relationship in the brain, across diverse spatiotemporal windows, not only at the global but also at the regional level [32], [34]. On the one hand, the joint consideration of measures of dynamics and synchronization may aid in the recognition of brain states, such as in relation to mental states and tasks. On the other, the establishment of a clear relationship between dynamics and synchronization across cortical regions could provide a new reference for assessing the integrity of brain function, with applications, for instance, in patients with discrete lesions or incipient degeneration [19], [31]. Extreme deviations from normal dynamics such as diffuse synchronization during epileptic seizures or reduced activity integration during coma are well-known pathological hallmarks; it should thus be seen whether more subtle deviations in the relationship between the complexity of node dynamics and connectivity convey useful information [18], [20], [31].

ACKNOWLEDGMENT

The authors are grateful to Daniel A Wagenaar, Steve M. Potter, and colleagues for providing neuronal cultures data. Preliminary research from which this work is partly derived was conducted while L. Minati was previously employed by the Istituto Neurologico Carlo Besta Foundation (Milano, Italy) and additionally funded by the Scienze Mente-Cervello Foundation (Rovereto, Italy).

REFERENCES

[1] M. E. J. Newman, "The structure and function of complex networks," *SIAM Rev.*, vol. 45, no. 2, pp. 167–256, May 2003.

[2] E. de Silva and M. P.H Stumpf, "Complex networks and simple models in biology," *J. Roy. Soc. Interface*, vol. 2, no. 5, pp. 419–430, Aug. 2005.

[3] D. Papo, J. M. Buldú, S. Boccaletti, and E. T. Bullmore, "Complex network theory and the brain," *Philos. Trans. Roy. Soc. B, Biol. Sci.*, vol. 369, Oct. 2014, Art. no. 20130520.

[4] L. A. Schintler, S. P. Gorman, A. Reggiani, R. Patuelli, A. Gillespie, P. Nijkamp, and J. Rutherford, "Complex network phenomena in telecommunication systems," *Netw. Spatial Econ.*, vol. 5, no. 4, pp. 351–370, Dec. 2005.

[5] K. Batool and M. A. Niazi, "Modeling the Internet of Things: A hybrid modeling approach using complex networks and agent-based models," *Complex Adapt. Syst. Model.*, vol. 5, no. 1, p. 4, Mar. 2017.

[6] M. Saleh, Y. Esa, and A. Mohamed, "Applications of complex network analysis in electric power systems," *Energies*, vol. 11, no. 6, p. 1381, May 2018.

[7] H. Leung, S. Chandana, and S. Wei, "Distributed sensing based on intelligent sensor networks," *IEEE Circuits Syst. Mag.*, vol. 8, no. 2, pp. 38–52, 2nd. Quart., 2008.

[8] F. Boschetti, M. Prokopenko, I. Macreadie, and A.-M. Grisogono, "Defining and detecting emergence in complex networks," in *Knowledge-Based Intelligent Information and Engineering Systems*. Berlin, Germany: Springer, 2005, pp. 573–580.

[9] S. Boccaletti, V. Latora, Y. Moreno, M. Chavez, and D.-U. Hwang, "Complex networks: Structure and dynamics," *Phys. Rep.*, vol. 424, nos. 4–5, pp. 175–308, Feb. 2006.

[10] L. M. Pecora and T. L. Carroll, "Master stability functions for synchronized coupled systems," *Phys. Rev. Lett.*, vol. 80, no. 10, pp. 2109–2112, Mar. 1998.

[11] A. Arenas, A. Díaz-Guilera, J. Kurths, Y. Moreno, and C. Zhou, "Synchronization in complex networks," *Phys. Rep.*, vol. 469, no. 3, pp. 93–153, Dec. 2008.

[12] L. M. Pecora, F. Sorrentino, A. M. Hagerstrom, T. E. Murphy, and R. Roy, "Cluster synchronization and isolated desynchronization in complex networks with symmetries," *Nature Commun.*, vol. 5, p. 4079, Jun. 2014.

[13] M. T. Schaub, N. O'Clery, Y. N. Billeh, J.-C. Delvenne, R. Lambiotte, and M. Barahona, "Graph partitions and cluster synchronization in networks of oscillators," *Chaos, Interdiscipl. J. Nonlinear Sci.*, vol. 26, no. 9, Aug. 2016, Art. no. 094821.

[14] Y.-Y. Liu, J.-J. Slotine, and A.-L. Barabási, "Controllability of complex networks," *Nature*, vol. 473, no. 7346, pp. 167–173, May 2011.

[15] S. P. Cornelius, W. L. Kath, and A. E. Motter, "Realistic control of network dynamics," *Nature Commun.*, vol. 4, p. 1942, Jun. 2013.

[16] D. A. B. Lombana and M. Di Bernardo, "Distributed PID control for consensus of homogeneous and heterogeneous networks," *IEEE Trans. Control Netw. Syst.*, vol. 2, no. 2, pp. 154–163, Jun. 2014.

[17] L. V. Gambuzza, M. Frasca, and V. Latora, "Distributed control of synchronization of a group of network nodes," *IEEE Trans. Autom. Control*, vol. 64, no. 1, pp. 365–372, Jan. 2019.

[18] A. Schnitzler and J. Gross, "Normal and pathological oscillatory communication in the brain," *Nature Rev. Neurosci.*, vol. 6, no. 4, pp. 285–296, Apr. 2005.

[19] M. I. Rabinovich, P. Varona, A. I. Selverston, and H. D. I. Abarbanel, "Dynamical principles in neuroscience," *Rev. Mod. Phys.*, vol. 78, pp. 1213–1265, Nov. 2006.

[20] M. I. Rabinovich, V. S. Afraimovich, C. Bick, and P. Varona, "Information flow dynamics in the brain," *Phys. Life Rev.*, vol. 9, no. 1, pp. 51–73, Mar. 2012.

[21] M. Kitsak, L. K. Gallos, S. Havlin, F. Liljeros, L. Muchnik, H. E. Stanley, and H. A. Makse, "Identification of influential spreaders in complex networks," *Nature Phys.*, vol. 6, pp. 888–893, Aug. 2010.

[22] L. Lü, D. Chen, X.-L. Ren, Q.-M. Zhang, Y.-C. Zhang, and T. Zhou, "Vital nodes identification in complex networks," *Phys. Rep.*, vol. 650, pp. 1–63, Sep. 2016.

[23] D. Dahmen, S. Grün, M. Diesmann, and M. Helias, "Second type of criticality in the brain uncovers rich multiple-neuron dynamics," *Proc. Nat. Acad. Sci. USA*, vol. 116, no. 26, pp. 13051–13060, Jun. 2019.

[24] S. Gu, F. Pasqualetti, M. Cieslak, Q. K. Telesford, A. B. Yu, A. E. Kahn, J. D. Medaglia, J. M. Vettel, M. B. Miller, S. T. Grafton, and D. S. Bassett, "Controllability of structural brain networks," *Nature Commun.*, vol. 6, p. 8414, Oct. 2015.

[25] F. Pasqualetti, S. Gu, and D. S. Bassett, "RE: Warnings and caveats in brain controllability," *NeuroImage*, vol. 197, pp. 586–588, Aug. 2019.

[26] Z. Gajic, M.-T. Lim, D. Skataric, W.-C. Su, and V. Kecman, *Optimal Control: Weakly Coupled Systems and Applications*. Boca Raton, FL, USA: CRC Press, 2008.

[27] A. E. Motter, C. Zhou, and J. Kurths, "Network synchronization, diffusion, and the paradox of heterogeneity," *Phys. Rev. E, Stat. Phys. Plasmas Fluids Relat. Interdiscip. Top.*, vol. 71, no. 1, Jan. 2005, Art. no. 016116.

[28] R. Hegger, H. Kantz, and T. Schreiber, "Practical implementation of nonlinear time series methods: The TISEAN package," *Chaos, Interdiscipl. J. Nonlinear Sci.*, vol. 9, p. 413, May 1999.

[29] T. Schreiber, "Measuring information transfer," *Phys. Rev. Lett.*, vol. 85, no. 2, p. 461, Jul. 2000.

[30] J. T. Lizier, *The Local Information Dynamics of Distributed Computation in Complex Systems*. Berlin, Germany: Springer-Verlag, 2012.

[31] C. J. Honey and O. Sporns, "Dynamical consequences of lesions in cortical networks," *Hum. Brain Mapping*, vol. 29, no. 7, pp. 802–809, Jul. 2008.

[32] M. Rubinov, O. Sporns, C. van Leeuwen, and M. Breakspear, "Symbiotic relationship between brain structure and dynamics," *BMC Neurosci.*, vol. 10, p. 55, Jun. 2009.

[33] L. Minati, P. Chiesa, D. Tabarelli, L. D'Incerti, and J. Jovicich, "Synchronization, non-linear dynamics and low-frequency fluctuations: Analogy between spontaneous brain activity and networked single-transistor chaotic oscillators," *Chaos, Interdiscipl. J. Nonlinear Sci.*, vol. 25, Mar. 2015, Art. no. 033107.

[34] J.-Y. Moon, U. Lee, S. Blain-Moraes, and G. A. Mashour, "General relationship of global topology, local dynamics, and directionality in large-scale brain networks," *PLoS Comput. Biol.*, vol. 11, no. 4, Apr. 2015, Art. no. e1004225.

[35] A. Tlaie, I. Leyva, R. Sevilla-Escoboza, V. P. Vera-Avila, and I. Sendiña-Nadal, "Dynamical complexity as a proxy for the network degree distribution," *Phys. Rev. E, Stat. Phys. Plasmas Fluids Relat. Interdiscip. Top.*, vol. 99, no. 1, Jan. 2019, Art. no. 012310.

[36] O. E. Rössler, "An equation for continuous chaos," *Phys. Lett. A*, vol. 57, no. 5, pp. 397–398, Jul. 1976.

[37] E. Ott, *Chaos in Dynamical Systems*. Cambridge, U.K.: Cambridge Univ. Press, 2002.

[38] A. Pikovsky, M. Rosenblum, and J. Kurths, *Synchronization: A Universal Concept in Nonlinear Sciences*. Cambridge, U.K.: Cambridge Univ. Press, 2003.

[39] R. Milo, S. Shen-Orr, S. Itzkovitz, N. Kashtan, D. Chklovskii, and U. Alon, "Network motifs: Simple building blocks of complex networks," *Science*, vol. 298, no. 5594, pp. 824–827, Oct. 2002.

[40] I. Fischer, R. Vicente, J. M. Buldú, M. Peil, C. R. Mirasso, M. C. Torrent, and J. García-Ojalvo, "Zero-lag long-range synchronization via dynamical relaying," *Phys. Rev. Lett.*, vol. 97, no. 12, Sep. 2006, Art. no. 123902.

[41] O. D'Huys, R. Vicente, T. Erneux, J. Danckaert, and I. Fischer, "Synchronization properties of network motifs: Influence of coupling delay and symmetry," *Chaos, Interdiscipl. J. Nonlinear Sci.*, vol. 18, no. 3, Sep. 2008, Art. no. 037116.

[42] A. Shilnikov, R. Gordon, and I. Belykh, "Polyrhythmic synchronization in bursting networking motifs," *Chaos, Interdiscipl. J. Nonlinear Sci.*, vol. 18, no. 3, Sep. 2008, Art. no. 037120.

[43] A. Bergner, M. Frasca, G. Sciuto, A. Buscarino, E. J. Ngamga, L. Fortuna, and J. Kurths, "Remote synchronization in star networks," *Phys. Rev. E, Stat. Phys. Plasmas Fluids Relat. Interdiscip. Top.*, vol. 85, no. 2, Feb. 2012, Art. no. 026208.

[44] C. Meena, K. Murali, and S. Sinha, "Chimera states in star networks," *Int. J. Bifurcation Chaos*, vol. 26, no. 9, May 2016, Art. no. 1630023.

[45] S. Krishnagopal, J. Lehnert, W. Poel, A. Zakharova, and E. Schöll, "Synchronization patterns: From network motifs to hierarchical networks," *Philos. Trans. Roy. Soc. B, Biol. Sci.*, vol. 375, no. 2088, Mar. 2017, Art. no. 20160216.

[46] L. F. Shampine and M. W. Reichelt, "The MATLAB ODE suite," *SIAM J. Sci. Comput.*, vol. 18, no. 1, pp. 1–22, 1997.

[47] F. Takens, "Detecting strange attractors in turbulence," in *Dynamical Systems and Turbulence, Warwick 1980* (Lecture Notes in Mathematics), vol. 898. New York, NY, USA: Springer, 1981, pp. 366–381.

[48] A. M. Fraser and H. L. Swinney, "Independent coordinates for strange attractors from mutual information," *Phys. Rev. A, Gen. Phys.*, vol. 33, no. 2, pp. 1134–1140, Feb. 1986.

[49] T. D. Sauer, J. A. Yorke, and M. Casdagli, "Embedology," *J. Statist. Phys.*, vol. 65, nos. 3–4, pp. 579–616, Nov. 1991.

[50] A. Provenzale, L. A. Smith, R. Vio, and G. Murante, "Distinguishing between low-dimensional dynamics and randomness in measured time series," *Physica D, Nonlinear Phenomena*, vol. 58, nos. 1–4, pp. 31–49, Sep. 1992.

[51] H. Kantz and T. Schreiber, *Nonlinear Time Series Analysis*. Cambridge, U.K.: Cambridge Univ. Press, 1997.

[52] P. Grassberger and I. Procaccia, "Measuring the strangeness of strange attractors," *Phys. D, Nonlinear Phenomena*, vol. 9, no. 1, pp. 189–208, Oct. 1983.

[53] L. Minati, "Experimental dynamical characterization of five autonomous chaotic oscillators with tunable series resistance," *Chaos, Interdiscipl. J. Nonlinear Sci.*, vol. 24, Jul. 2014, Art. no. 033110.

[54] K. P. Michalak, "How to estimate the correlation dimension of high-dimensional signals?" *Chaos, Interdiscipl. J. Nonlinear Sci.*, vol. 24, no. 3, Jul. 2014, Art. no. 033118.

[55] L. Minati, M. Frasca, G. Giustolisi, P. Oświęcimka, S. Drożdż, and L. Ricci, "High-dimensional dynamics in a single-transistor oscillator containing Feynman-Sierpiński resonators: Effect of fractal depth and irregularity," *Chaos, Interdiscipl. J. Nonlinear Sci.*, vol. 28, Sep. 2018, Art. no. 093112.

[56] C. Bandt and B. Pompe, "Permutation entropy: A natural complexity measure for time series," *Phys. Rev. Lett.*, vol. 88, no. 17, Apr. 2002, Art. no. 174102.

[57] M. Riedl, A. Muüller, and N. Wessel, "Practical considerations of permutation entropy," *Eur. Phys. J. Special Topics*, vol. 222, no. 2, pp. 249–262, Jun. 2013.

[58] B. Sivakumar, "Rainfall dynamics at different temporal scales: A chaotic perspective," *Hydrol. Earth Syst. Sci. Discuss.*, vol. 5, pp. 645–652, Dec. 2001.

[59] M. T. Martin, A. Plastino, and O. A. Rosso, "Statistical complexity and disequilibrium," *Phys. Lett. A*, vol. 311, nos. 2–3, pp. 126–132, May 2003.

[60] P. W. Lamberti, M. T. Martin, A. Plastino, and O. A. Rosso, "Intensive entropic non-triviality measure," *Phys. A, Stat. Mech. Appl.*, vol. 334, nos. 1–2, pp. 119–131, Mar. 2004.

[61] S. Boccaletti, J. Kurths, G. Osipov, D. L. Valladares, and C. S. Zhou, "The synchronization of chaotic systems," *Phys. Rep.*, vol. 366, nos. 1–2, pp. 1–101, Aug. 2002.

[62] H.-F. Zhang, R.-X. Wu, and X.-C. Fu, "The emergence of chaos in complex dynamical networks," *Chaos, Solitons Fractals*, vol. 28, no. 2, pp. 472–479, Apr. 2006.

[63] J. G. Barajas-Ramírez, and R. Femat, "On the emergence of chaos in dynamical networks," *Int. J. Syst. Sci.*, vol. 43, no. 12, pp. 2240–2248, May 2011.

[64] J. T. Lizier and M. Prokopenko, "Differentiating information transfer and causal effect," *Eur. Phys. J. B*, vol. 73, no. 4, pp. 605–615, Feb. 2010.

[65] L. Faes, D. Kugiumtzis, G. Nollo, F. Jurysta, and D. Marinazzo, "Estimating the decomposition of predictive information in multivariate systems," *Phys. Rev. E, Stat. Phys. Plasmas Fluids Relat. Interdiscip. Top.*, vol. 91, no. 3, Mar. 2015, Art. no. 032904.

[66] L. F. Kozachenko and N. N. Leonenko, "Sample estimate of the entropy of a random vector," *Problemy Peredachi Inform.*, vol. 23, no. 2, pp. 9–16, 1987.

[67] A. Kraskov, H. Stögbauer, and P. Grassberger, "Estimating mutual information," *Phys. Rev. E, Stat. Phys. Plasmas Fluids Relat. Interdiscip. Top.*, vol. 69, no. 6, Jun. 2004, Art. no. 066138.

[68] Z. Ma, G. Zhang, Y. Wang, and Z. Liu, "Cluster synchronization in star-like complex networks," *J. Phys. A, Math. Theor.*, vol. 41, no. 15, Apr. 2008, Art. no. 155101.

[69] L. Minati, L. Faes, M. Frasca, P. Oświęcimka, and S. Drożdż, "Apparent remote synchronization of amplitudes: A demodulation and interference effect," *Chaos, Interdiscipl. J. Nonlinear Sci.*, vol. 28, no. 6, Jun. 2018, Art. no. 063124.

[70] M. Newman, *Networks: An Introduction*. Oxford U.K.: Oxford Univ. Press, 2010.

[71] R. Albert and A.-L. Barabási, "Statistical mechanics of complex networks," *Rev. Mod. Phys.*, vol. 74, no. 47, pp. 47–97, Jan. 2002.

[72] V. Latora, V. Nicosia, and G. Russo, *Complex Networks: Principles, Methods and Applications*. Cambridge, U.K.: Cambridge Univ. Press, 2017.

[73] A. Perinelli and L. Ricci, "Identification of suitable embedding dimensions and lags for time series generated by chaotic, finite-dimensional systems," *Phys. Rev. E, Stat. Phys. Plasmas Fluids Relat. Interdiscip. Top.*, vol. 98, Nov. 2018, Art. no. 052226.

[74] L. Minati, J. Winkel, A. Bifone, P. Oświęcimka, and J. Jovicich, "Self-similarity and quasi-idempotence in neural networks and related dynamical systems," *Chaos, Interdiscipl. J. Nonlinear Sci.*, vol. 27, Apr. 2017, Art. no. 043115.

[75] S.-H. Yook and H. Meyer-Ortmanns, "Synchronization of Rössler oscillators on scale-free topologies," *Phys. A, Stat. Mech. Appl.*, vol. 371, no. 2, pp. 781–789, Nov. 2006.

[76] T. Saito, "An approach toward higher dimensional hysteresis chaos generators," *IEEE Trans. Circuits Syst.*, vol. 37, no. 3, pp. 399–409, Mar. 1990.

[77] A. Buscarino, L. Fortuna, and M. Frasca, *Essentials of Nonlinear Circuit Dynamics with MATLAB and Laboratory Experiments*. Boca Raton, FL, USA: CRC Press, 2017.

[78] L. Minati, "Across neurons and silicon: Some experiments regarding the pervasiveness of nonlinear phenomena," *Acta Phys. Pol. B*, vol. 49, no. 12, pp. 2029–2094, Dec. 2018.

[79] *Publicly Available Data*. Accessed: Oct. 4, 2019. [Online]. Available: http://www.lminati.it/listing/2019/d/
[80] J. D. Johnston, "Transform coding of audio signals using perceptual noise criteria," *IEEE J. Sel. Areas Commun.*, vol. 6, no. 2, pp. 314–323, Feb. 1988.
[81] L. Minati, M. Frasca, P. Oświęcimka, L. Faes, and S. Drożdż, "Atypical transistor-based chaotic oscillators: Design, realization, and diversity," *Chaos, Interdiscipl. J. Nonlinear Sci.*, vol. 27, no. 7, Jul. 2017, Art. no. 073113.
[82] E. T. Rolls and G. Deco, *The Noisy Brain: Stochastic Dynamics as a Principle of Brain*. Oxford U.K.: Oxford Univ. Press, 2010.
[83] P. Sibani and H. J. Jensen, *Stochastic Dynamics of Complex Systems: From Glasses to Evolution*. London, U.K.: Imperial College Press, 2013.
[84] D. Tabarelli, A. Vilardi, C. Begliomini, F. Pavani, M. Turatto, and L. Ricci, "Statistically robust evidence of stochastic resonance in human auditory perceptual system," *Eur. Phys. J. B*, vol. 69, no. 1, pp. 155–159, May 2009.
[85] L. Gammaitoni, P. Hänggi, P. Jung, and F. Marchesoni, "Stochastic resonance," *Rev. Mod. Phys.*, vol. 70, no. 1, pp. 223–287, Jan. 1998.
[86] M. D. McDonnell and L. M. Ward, "The benefits of noise in neural systems: Bridging theory and experiment," *Nature Rev. Neurosci.*, vol. 12, no. 7, pp. 415–425, Jun. 2011.
[87] K. Chen, P. Bak, and S. P. Obukhov, "Self-organized criticality in a crack-propagation model of earthquakes," *Phys. Rev. A, Gen. Phys.*, vol. 43, no. 2, pp. 625–630, Jan. 1991.
[88] B. Drossel and F. Schwabl, "Self-organized critical forest-fire model," *Phys. Rev. Lett.*, vol. 69, no. 11, pp. 1629–1632, Sep. 1992.
[89] A. N. Burkitt, "A review of the integrate-and-fire neuron model: II. Inhomogeneous synaptic input and network properties," *Biol Cybern.*, vol. 95, no. 2, pp. 97–112, Aug. 2006.
[90] L. Minati, A. de Candia, and S. Scarpetta, "Critical phenomena at a first-order phase transition in a lattice of glow lamps: Experimental findings and analogy to neural activity," *Chaos, Interdiscipl. J. Nonlinear Sci.*, vol. 27, no. 7, Jun. 2016, Art. no. 073103.
[91] M. A. Muñoz, "*Colloquium*: Criticality and dynamical scaling in living systems," *Rev. Mod. Phys.*, vol. 90, Jul. 2018, Art. no. 031001.
[92] D. J. Daley and D. Vere-Jones, *An Introduction to the Theory of Point Processes: Elementary Theory and Methods*, vol. I. Berlin, Germany: Springer, 2006.
[93] W. Truccolo, "From point process observations to collective neural dynamics: Nonlinear Hawkes process GLMs, low-dimensional dynamics and coarse graining," *J. Physiol.-Paris*, vol. 110, no. 4, pp. 336–347, Nov. 2016.
[94] T. J. Lewis and J. Rinzel, "Dynamics of spiking neurons connected by both inhibitory and electrical coupling," *J. Comput. Neurosci.*, vol. 14, no. 3, pp. 283–309, May 2003.
[95] A. C. Skeldon, D.-J. Dijk, and G. Derks, "Mathematical models for sleep-wake dynamics: Comparison of the two-process model and a mutual inhibition neuronal model," *PLoS ONE*, vol. 9, no. 8, Aug. 2014, Art. no. e103877.
[96] M. Koyama and A. Pujala, "Mutual inhibition of lateral inhibition: A network motif for an elementary computation in the brain," *Current Opinion Neurobiol.*, vol. 49, pp. 69–74, Apr. 2018.
[97] L. Zunino and C. W. Kulp, "Detecting nonlinearity in short and noisy time series using the permutation entropy," *Phys. Lett. A*, vol. 381, no. 42, pp. 3627–3635, Nov. 2017.
[98] T. Schreiber and A. Schmitz, "Improved surrogate data for nonlinearity tests," *Phys. Rev. Lett.*, vol. 77, no. 4, pp. 635–638, Jul. 1996.
[99] V. Pasquale, P. Massobrio, L. L. Bologna, M. Chiappalone, and S. Martinoia, "Self-organization and neuronal avalanches in networks of dissociated cortical neurons," *Neuroscience*, vol. 153, no. 4, pp. 1354–1369, Jun. 2008.
[100] J. A. Kromer, L. Schimansky-Geier, and A. B. Neiman, "Emergence and coherence of oscillations in star networks of stochastic excitable elements," *Phys. Rev. E, Stat. Phys. Plasmas Fluids Relat. Interdiscip. Top.*, vol. 93, no. 4, Apr. 2016, Art. no. 042406.
[101] F. O. Morin, Y. Takamura, and E. Tamiya, "Investigating neuronal activity with planar microelectrode arrays: Achievements and new perspectives," *J. Biosci. Bioeng.*, vol. 100, no. 2, pp. 131–143, Aug. 2005.
[102] D. A. Wagenaar, J. Pine, and S. M. Potter, "An extremely rich repertoire of bursting patterns during the development of cortical cultures," *BMC Neurosci.*, vol. 7, p. 11, Feb. 2006.
[103] *Publicly Available Data*. Accessed: Oct. 4, 2019. [Online]. Available: http://potterlab.bme.gatech.edu/development-data/html/index.html
[104] C. S. Cutts and S. J. Eglen, "Detecting pairwise correlations in spike trains: An objective comparison of methods and application to the study of retinal waves," *J. Neurosci.*, vol. 34, no. 43, pp. 14288–14303, Oct. 2014.
[105] J. H. Downes, M. W. Hammond, D. Xydas, M. C. Spencer, V. M. Becerra, K. Warwick, B. J. Whalley, and S. J. Nasuto, "Emergence of a small-world functional network in cultured neurons," *PLoS Comput Biol.*, vol. 8, May 2012, Art. no. e1002522.
[106] J. M. Beggs and D. Plenz, "Neuronal avalanches in neocortical circuits," *J. Neurosci.*, vol. 23, no. 35, pp. 11167–11177, Dec. 2003.
[107] W. Chen, X. Li, J. Pu, and Q. Luo, "Spatial-temporal dynamics of chaotic behavior in cultured hippocampal networks," *Phys. Rev. E, Stat. Phys. Plasmas Fluids Relat. Interdiscip. Top.*, vol. 81, no. 6, Jun. 2010, Art. no. 061903.
[108] N. Tabareau, J.-J. Slotine, and Q.-C. Pham, "How synchronization protects from noise," *PLoS Comput. Biol.*, vol. 6, Jan. 2010, Art. no. e1000637.
[109] E. Brewer and J. W. C. Tomlinson, "The manager's working day," *J. Ind. Econom.*, vol. 12, no. 3, pp. 191–197, Jul. 1964.
[110] L. K. Kana, A. Fomethe, H. B. Fotsin, E. T. Wembe, and A. I. Moukengue, "Complex dynamics and synchronization in a system of magnetically coupled colpitts oscillators," *J. Nonlinear Dyn.*, vol. 2017, Apr. 2017, Art. no. 5483956.
[111] M. Pontón, and A. Suárez, "Stability analysis of wireless coupled-oscillator circuits," in *IEEE MTT-S Int. Microw. Symp. Dig.*, Honolulu, HI, USA, Jun. 2017, pp. 83–86.
[112] Y.-Y. Lui and A.-L. Barabási, "Control principles of complex systems," *Rev. Mod. Phys.*, vol. 88, no. 3, Sep. 2016, Art. no. 035006.
[113] P. DeLellis, F. Garofalo, and F. Lo Iudice, "The partial pinning control strategy for large complex networks," *Automatica*, vol. 89, pp. 111–116, Mar. 2018.
[114] E. Schöll and H. G. Schuster, *Handbook of Chaos Control*, vol. 2. Hoboken, NJ, USA: Wiley, 2008.
[115] J. Cabral, M. L. Kringelbach, and G. Deco, "Exploring the network dynamics underlying brain activity during rest," *Prog. Neurobiol.*, vol. 114C, pp. 102–131, Mar. 2014.

LUDOVICO MINATI (A'00–M'04–SM'13) received the B.S. degree in information technology and computing and the M.S. degree in science from The Open University, Milton Keynes, U.K., in 2004 and 2006, respectively, the M.S. degree in applied cognitive neuroscience from the University of Westminster, London, U.K., in 2008, the B.S. degree in physical science and the M.S. degree in medical physics from The Open University, in 2009, the Ph.D. degree in neuroscience from the Brighton and Sussex Medical School, U.K., in 2012, and the D.Sc. (doktor habilitowany) degree in physics from the Institute of Nuclear Physics—Polish Academy of Sciences, Kraków, Poland, in 2017.

He has held research and consulting roles across public institutions and private companies, including the Institute of Nuclear Physics—Polish Academy of Sciences, the Carlo Besta Neurological Institute, Milan, Italy, and the Brighton and Sussex Medical School. He has authored over 120 articles and five patents. He is currently a Specially Appointed Associate Professor with the Institute of Innovative Research, Tokyo Institute of Technology, Japan, an Affiliate with the Center for Mind/Brain Sciences, University of Trento, Italy, and a Freelance Research and Development Consultant. His research interests include non-linear dynamical systems, chaotic oscillators, reconfigurable analog and digital computing, functional magnetic resonance imaging, advanced techniques for bio-signal analysis, brain machine/computer interfaces, and robotics.

Dr. Minati is also a Chartered Engineer and a member with the Institution of Engineering and Technology, U.K, a Chartered Physicist and a member with the Institute of Physics, London, and a Chartered Scientist and a member with the Institute of Physics and Engineering in Medicine, York, U.K. He is also a member with the Institute of Electronics, Information, and Communication Engineers (IEICE) and the Japan Neuroscience Society.

HIROYUKI ITO (S'03–M'04) received the B.E. degree from the Department of Electronics and Mechanical Engineering, Chiba University, Chiba, Japan, in 2002, and the M.E. and Ph.D. degrees from the Department of Advanced Applied Electronics, Tokyo Institute of Technology, Yokohama, Japan, in 2004 and 2006, respectively.

From 2004 to 2007, he was a Research Fellow of the Japan Society for the Promotion of Science. He was a temporary Visiting Researcher and a Visiting Professor with the Communications Technology Laboratory, Intel Corporation, Hillsboro, OR, USA, from 2006 to 2007. He was an Assistant Professor with the Precision and Intelligence Laboratory, Tokyo Institute of Technology, from 2007 to 2013, where he was an Associate Professor, from 2013 to 2015. From 2008 to 2010, he was with Fujitsu Laboratories Ltd., Yokohama, where he developed an RF CMOS transceiver and digital calibration techniques for mobile-WiMAX application. Since 2016, he has been an Associate Professor with the Institute of Innovative Research, Tokyo Institute of Technology. His research interests include analog, RF and mixed-signal circuit design for the IoT, and their application. He is a member of the IEEE Solid-State Circuits Society, the Institute of Electronics, the Information and Communication Engineers (IEICE), and the Japan Society of Applied Physics (JSAP).

ALESSIO PERINELLI received the B.S. and M.S. degrees in physics from the University of Trento, in 2015 and 2017, respectively, where he is currently pursuing the Ph.D. degree in physics with the Nonlinear Systems and Electronics Laboratory, Department of Physics. His research interests concern the investigation of nonlinear and chaotic systems, the development of nonlinear time series analysis methods, and the application of nonlinear methods to signals generated by the human brain.

LEONARDO RICCI (M'18) received the M.S. degree in physics from the University of Pisa, Pisa, Italy, in 1990, and the Ph.D. degree in physics from the Ludwig-Maximilian Universität, Munich, Germany, in 1994. From 1990 to 1994, he worked with T. W. Hänsch's Group, Munich. In 1995, he moved to the Department of Physics, University of Trento, Trento, Italy, where is currently an Adjunct Professor. His research interests mainly concern the investigation of the role of noise in brain function, nonlinear dynamics, and the development of nonlinear techniques for time series analysis.

LUCA FAES received the M.S. degree in electronic engineering from the University of Padova, Italy, in 1998, and the Ph.D. degree in electronic devices from the University of Trento, Italy, in 2003.

He is currently working as an Associate Professor with the Department of Engineering, University of Palermo, and the BIOtech Center, Department of Industrial Engineering, University of Trento. His research pertains to the development of methods for time series analysis and system modeling, with applications to cardiovascular neuroscience, cardiac arrhythmias, brain connectivity, and physiological networks. He has authored five book chapters and more than 150 publications in these fields. He is a member of the Italian Society of Chaos and Complexity, the IEEE Engineering in Medicine and Biology Society, the European Study Group on Cardiovascular Oscillations, and the Italian National Bioengineering Group.

NATSUE YOSHIMURA received the M.S. degree from Tokyo Medical and Dental University, Japan, in 2006, and the Ph.D. degree from The University of Electro-Communications, Japan, in 2009.

She was a Postdoctoral Researcher with the Tokyo Institute of Technology, from 2009 to 2010, where she became an Assistant Professor. She has been an Associate Professor with the Institute of Innovative Research, Tokyo Institute of Technology, since 2015. She is currently a Visiting Researcher with the Integrative Brain Imaging Center and the National Center of Neurology and Psychiatry. Her research interests include brain machine/computer interfaces, brain activity information decoding relating to motor control, speech, and emotion, using noninvasive brain activity recording methods, such as electroencephalography and functional magnetic resonance imaging. She is a member of the Society for Neuroscience, the Japan Neuroscience Society, and the Japanese Society for Medical and Biological Engineering.

YASUHARU KOIKE received the B.S., M.S., and Ph.D. degrees in engineering from the Tokyo Institute of Technology, Tokyo, Japan, in 1987, 1989, and 1996, respectively.

From 1989 to 1998, he was with Toyota Motor Corporation. From 1991 to 1994, he transferred to the Advanced Tele-communications Research Human Information Processing Laboratories, Kyoto, Japan. In 1998, he moved to the Precision and Intelligence Laboratory, Tokyo Institute of Technology, where he is currently a Professor with the Institute of Innovative Research. He was a Researcher of the Precursory Research for Embryonic Science and Technology, Japan Science and Technology Corporation, from 2000 to 2004, and CREST, JST, from 2004 to 2014. His research interests include human motor control theory, human interface, and brain machine interface and their applications.

Dr. Koike is a member of the Society for Neuroscience, the Institute of Electronics, Information and Communication Engineers (IEICE), the Virtual Reality Society of Japan, and the Japan Neuroscience Society.

MATTIA FRASCA (M'00–SM'09) received the degree in electronics engineering and the Ph.D. degree in electronics and automation engineering from the University of Catania, Italy, in 2000 and 2003, respectively.

He is currently an Associate Professor and teaches process control and complex systems with the University of Catania. He has authored or coauthored six books and over 250 articles on refereed international journals and proceedings. He is also a coauthor of two international patents. His scientific interests include nonlinear systems and chaos, complex networks, and bio-inspired robotics.

Dr. Frasca was one of the Organizers of the Tenth Experimental Chaos Conference, the Co-Chair of the Fourth International Conference on Physics and Control and the Chair of the European Conference on Circuit Theory and Design, in 2017. He is also the President of the Italian Society for Chaos and Complexity. He has served as an Associate Editor for the IEEE TRANSACTIONS ON CIRCUITS AND SYSTEMS I, from 2012 to 2015. He is also an Associate Editor of the *Journal of Complex Networks* and an Editor of *Chaos, Solitons, and Fractals*.